As explained earlier, when the AMT method and the dipole-dipole method are compared, the AMT method is more sensitive to the resistivity structure of the deep zone, but the dipole-dipole method is more sensitive to the resistivity structure of the shallow zone. Also, with the AMT method the influence of the local resistivity structure of the shallow zone affects interpretation of the deep zone, but with the dipole-dipole method there is little effect. By conducting interpretation using the two types of measurement data with their different characteristics at the same time, in the shallow zone the dipole-dipole method takes preference which has high sensitivity to the resistivity structure of the shallow zone, while in the deep zone the AMT method is used effectively which has high sensitivity to the resistivity structure of the deep zone. Furthermore, compared with interpretation by AMT alone, as the detailed structure of the shallow zone can be meaningfully obtained, the possibility of the local resistivity structure of the shallow zone affecting the deep zone is reduced and as a result an accurate interpretation from the shallow zone to the deep zone is possible.

As for the resistivity blocks for two-dimensional joint inversion interpretation, in the shallow zone up to a depth of 500m a resistivity block boundary was set for each electrode, in the same way as for two-dimensional inversion interpretation by the IP method, and below 500m a resistivity block was set at each measurement point, in the same way as for two-dimensional inversion interpretation by the AMT method. These were then deformed to suit the topography of the surface and interpretation which included the topographical effects was carried out.

3-3 Measurement Results and Interpretation Results

3-3-1 Measurement Results

1. AMT Measurement Results

Pseudosections of the apparent resistivity and phase difference at each profile taking the vertical axis as the measurement frequency are shown in Fig.II-3-6(1) - Fig.II-3-6(5).

Considering the AMT measurement results from the viewpoint of the apparent resistivity pseudosections, with the exception of Profile I, there are many data that suggest the influence of topography , and a low resistivity anomaly zone in only the shallow zone, etc. For example, the measurement point most strongly affected by mountainous terrain is profile II measurement point 600, and the measurement values must be made about 3 times greater to achieve terrain correction. Also, the measurement point most affected by the influence of valley terrain is profile III measurement point 1000, and the values must be made about 0.3 times greater.

The topographical and static effects on each profile are described below.

Profile I (Fig.II-3-6(1))

The topography is virtually horizontal and there are no effect of topograpy and static shift.

Profile II (Fig.II-3-6(2))

The effects of the mountainous terrain can be seen at measurement point 600 and of the valley terrain at measurement point 800. Also, the apparent resistivity is lower from measurement point 200 to measurement point 800 than at measurement point 1000, but as there is virtually no change in the phase difference up to measurement point 1000 especially in the shallow zone (high frequency zone), the influence of static effect is assumed.

Profile III (Fig.II-3-6(3))

This is the profile with the most drastic changes in topography and the effects of the mountainous terrain are seen at measurement points 200 and 900, while the effects of the valley terrain are seen at measurement points 1000 and 1400. Measurement point 600 shows higher apparent resistivity than neighboring measurement points, but as there is no change in the phase difference section, static effect due to a local high resistivity zone is assumed.

Profile IV (Fig.II-3-6(4))

The effects of the mountainous terrain are seen at measurement point 2200 and of the valley terrain at measurement point 2400. Also, the influence of static effect due to a low resistivity zone in the shallow zone is presumed from measurement point 200 to 1200, and from measurement point 2000 to 2200.

Profile V (Fig.II-3-6(5))

The influence of mountainous terrain is seen at measurement points 600 and 800. And the influence of static effect is assumed at measurement points 800 and 1000.

As described above, topographical and static effects are very apparent in the survey area and it is impossible to estimate the resistivity structure of the area directly from the apparent resistivity pseudosections. Similarly, when Bostic inversion interpretation and one-dimensional interpretation are applied without evaluating the above effects, it results in a false image of local high resistivity or low resistivity and the correct resistivity structure cannot be obtained. For this reason, to examine the resistivity structure of the survey area, it is necessary to carry out two-dimensional inversion interpretation which takes into account the topography and two-dimensional joint inversion interpretation using both the AMT method and the IP method.

2. IP Measurement Results

The measured apparent resistivity and chargeability are shown in the pseudosections in Fig.II-3-7(1) - Fig.II-3-7(5). The rough quantitative apparent resistivity structure and chargeability of each profile according to the IP pseudosections are described below.

Profile I (Fig.II-3-7(1))

A virtual horizontally multi-layered structure is assumed and the apparent resistivity values become lower from the shallow zone (approx. 200 Ωm) to the deep zone (approx. 60 Ωm). Chargeability becomes

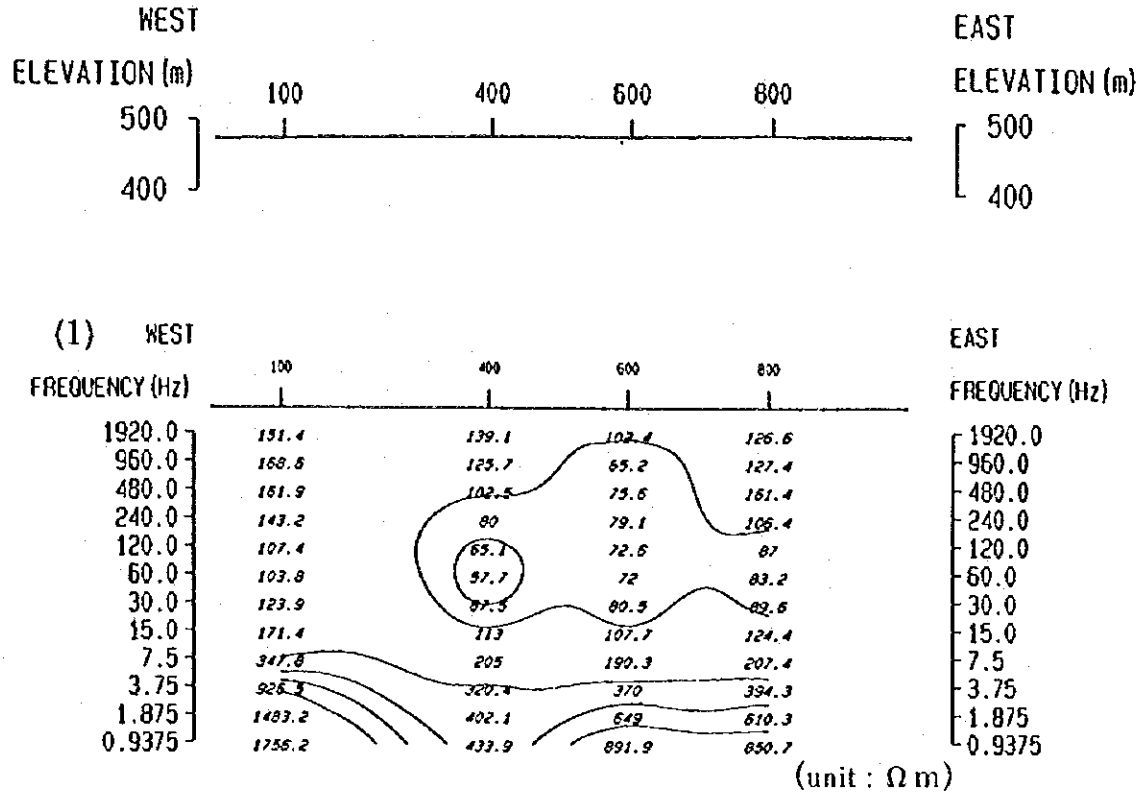

100 0 100 200 300 (m)

Fig. II-3-6(1)

Pseudosection of apparent resistivity(1) and phase (2) difference for profile I

(1 : 10,000)

Geophysical Survey (AMT), Phase II

Progreso Project, JICA/MMAJ-ENAMI

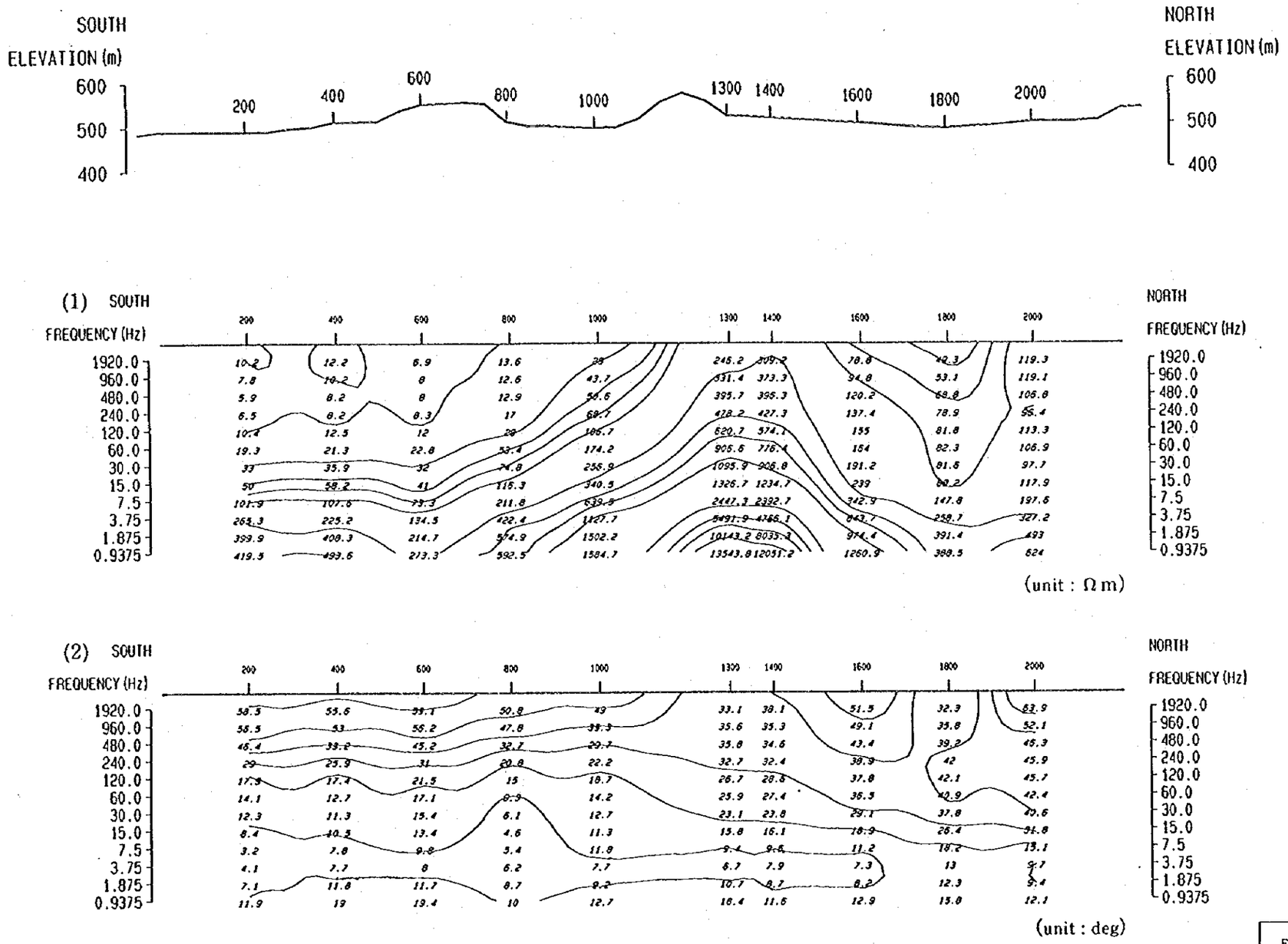

Fig II-3-6(2)

Pseudosection of apparent resistivity(1) and phase(2) difference for profile II

(1 : 10,000)

Geophysical Survey (AMT), Phase II

Progreso Project, JICA/MMAJ-ENAMI

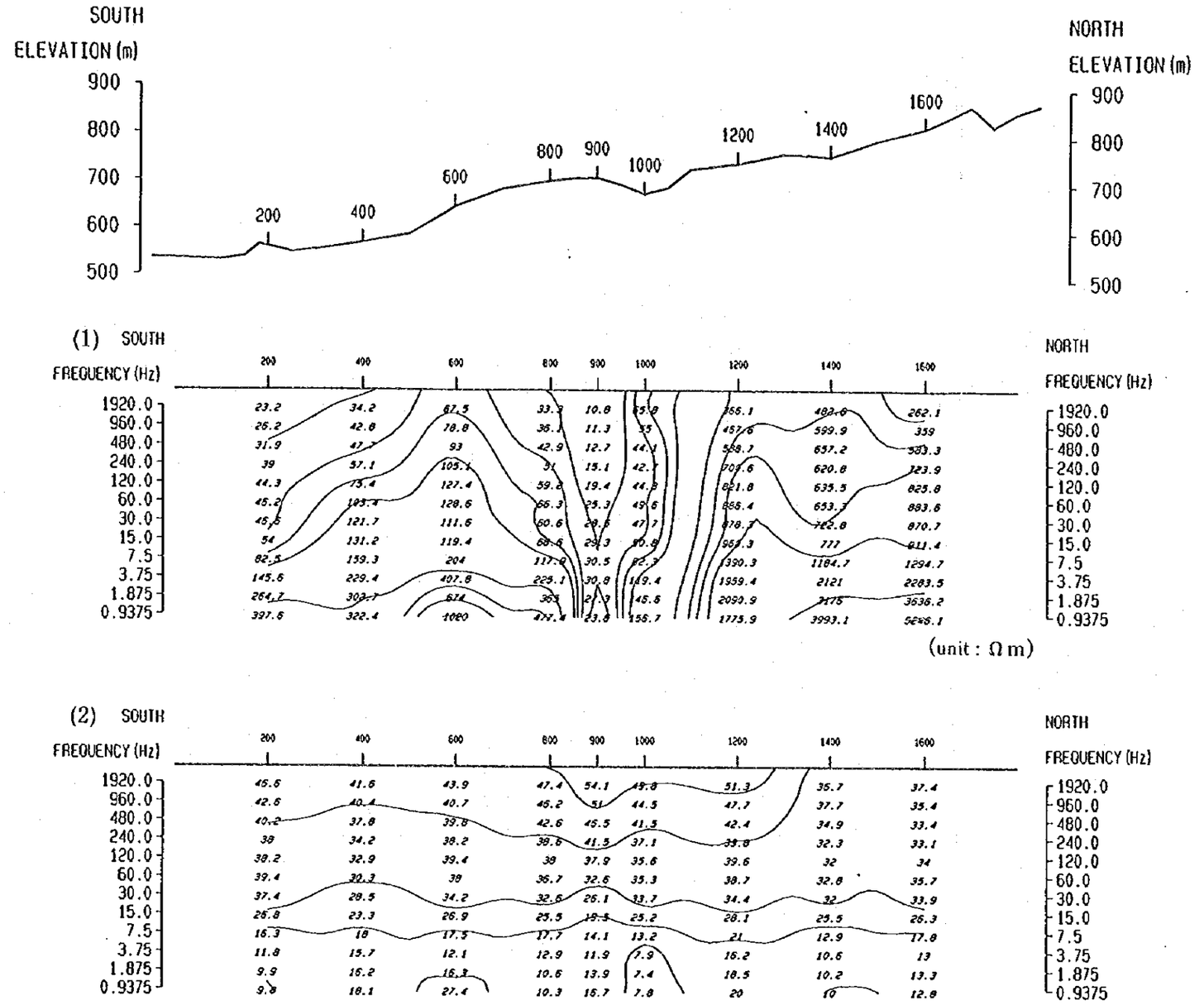

Fig. II-3-6(3)

Pseudosection of apparent resistivity(1) and phase(2) difference for profile III

(1 : 10,000)

Geophysical Survey (AMT), Phase II

Progreso Project, JICA/MMAJ-ENAMI

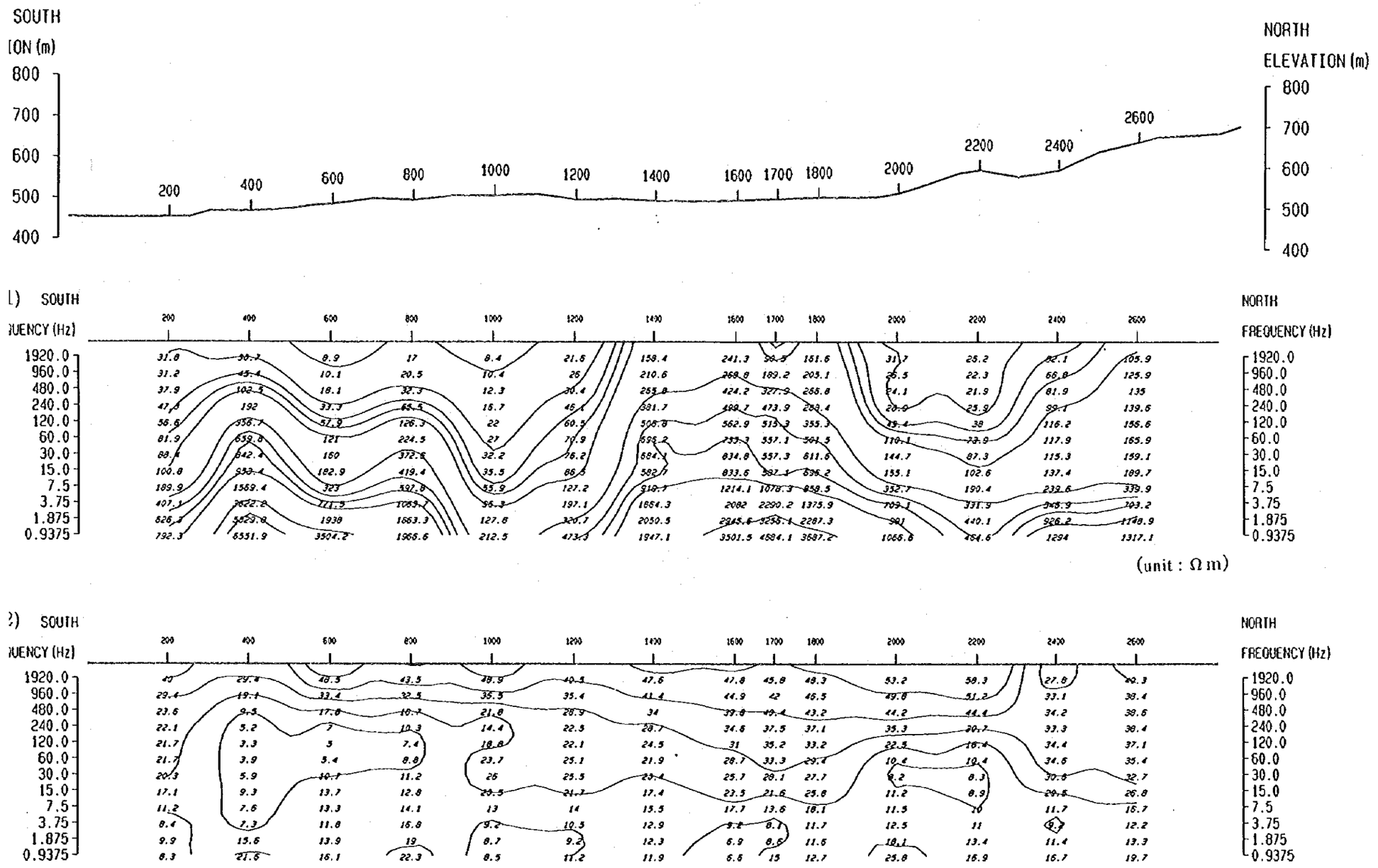

Fig. II-3-6(4)

Pseudosection of apparent resistivity(1) and phase(2) difference for profile IV

(1 : 10,000)

Geophysical Survey (AMT), Phase II

Progreso Project, JICA/MMAJ-ENAMI

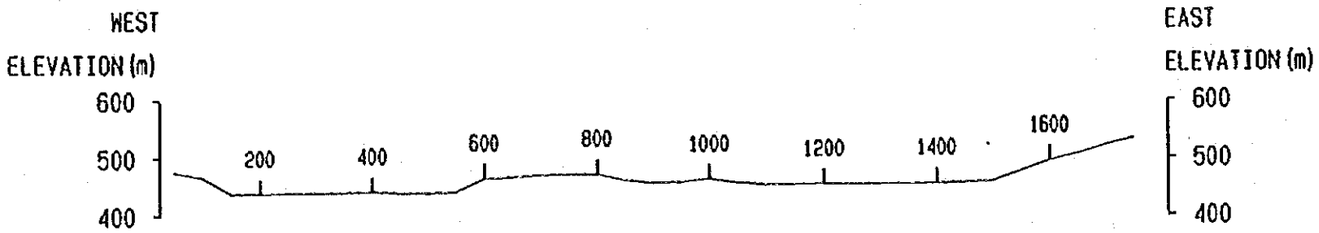

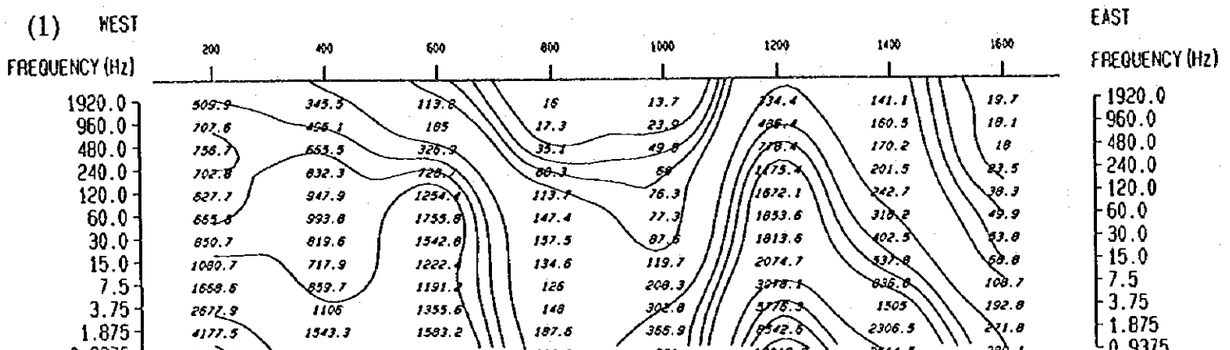

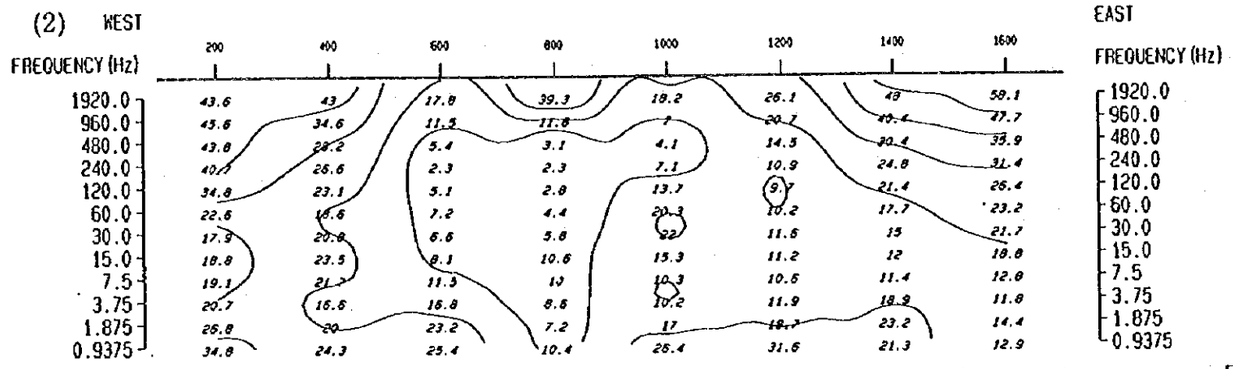

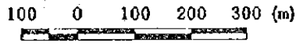

Fig. II-3-6(5)

Pseudosection of apparent resistivity(1) and phase(2) difference for profile V

(1 : 10,000)

Geophysical Survey (AMT), Phase II

Progreso Project, JICA/MMAJ-ENAMI

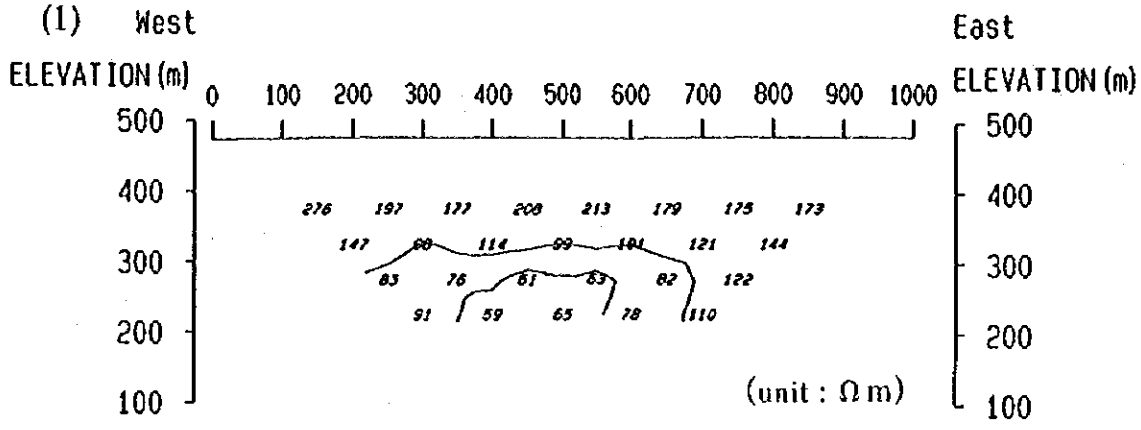

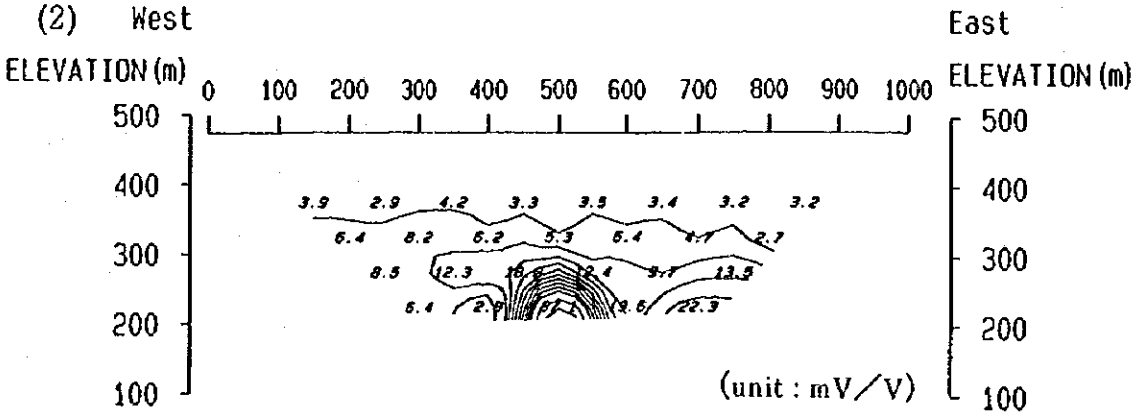

Fig. II-3-7(1)

Pseudosection of apparent resistivity(1) and chargeability(2) for profile I

(1 : 10,000)

Geophysical Survey (IP), Phase II

Progreso Project, JICA/MMAJ-ENAMI

(1) South

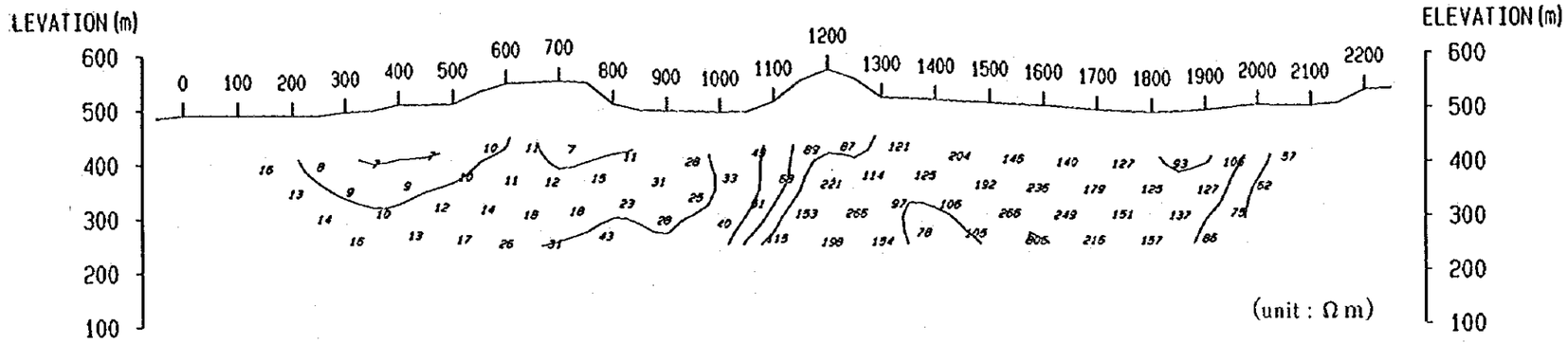

North

(2) South

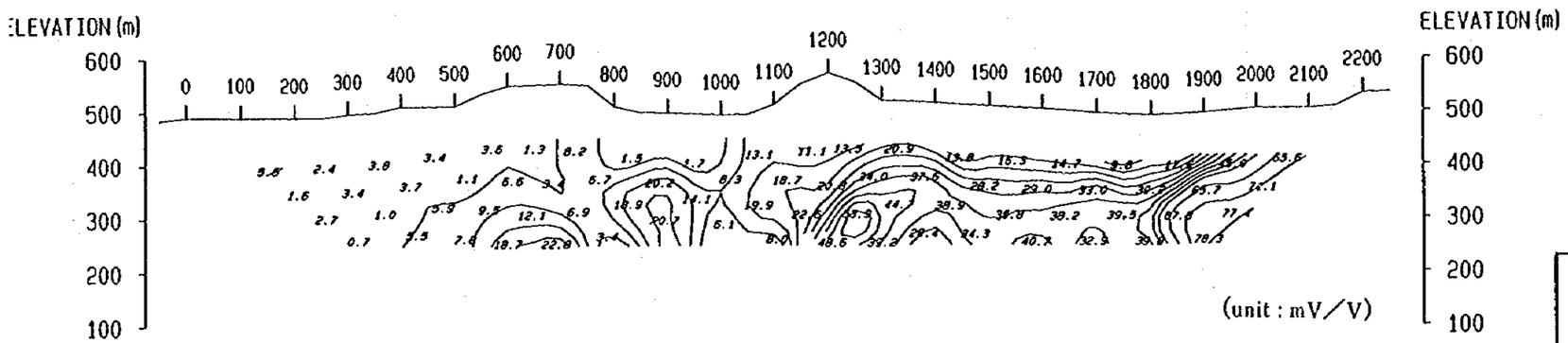

North

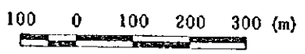

Fig. II-3-7(2)

Pseudosection of apparent resistivity(1) and chargeability(2) for profile II

(1 : 10,000)

Geophysical Survey (IP), Phase II

Progreso Project, JICA/MMAJ-ENAMI

(1) South

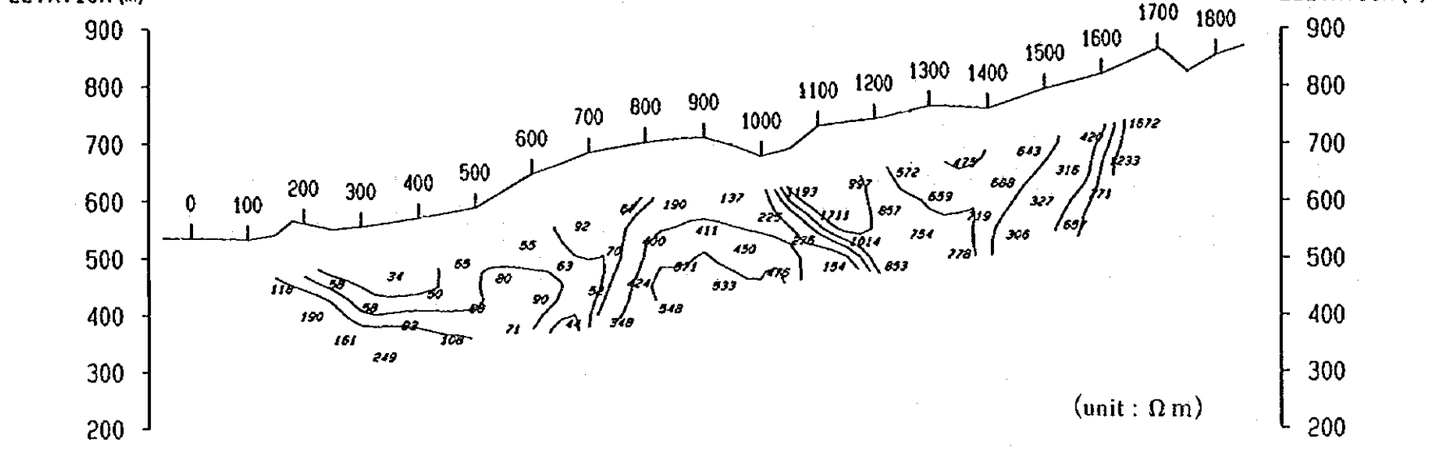

North

ELEVATION (m)

(2) South

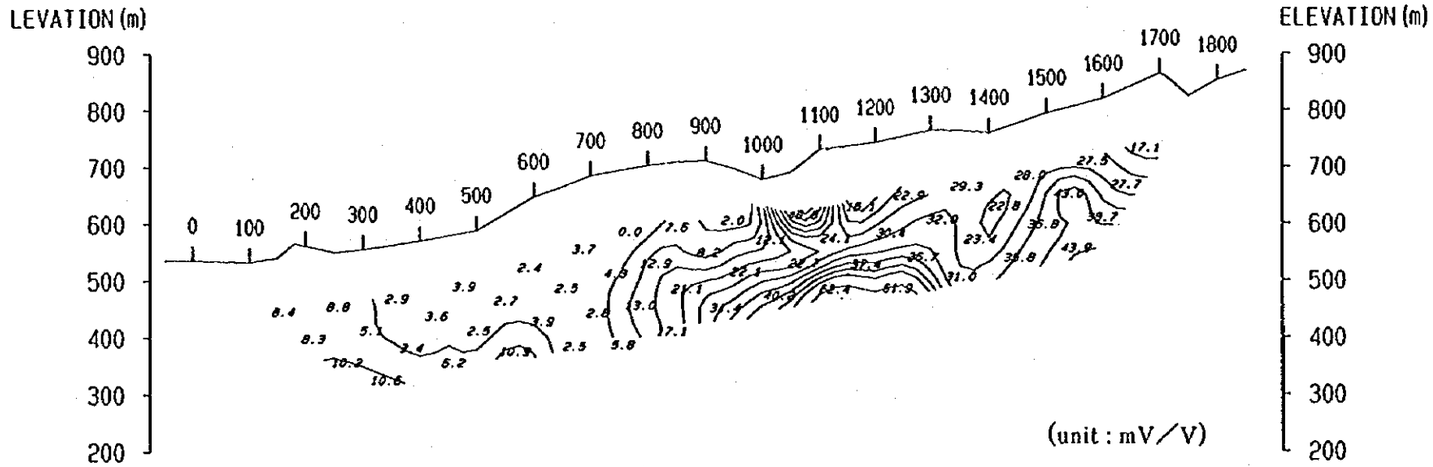

North

ELEVATION (m)

100 0 100 200 300 (m)

Fig. II-3-7(3)

Pseudosection of apparent resistivity(1) and chargeability(2) for profile III

(1 : 10,000)

Geophysical Survey (IP), Phase II

Progreso Project, JICA/MMAJ-ENAMI

(1) South

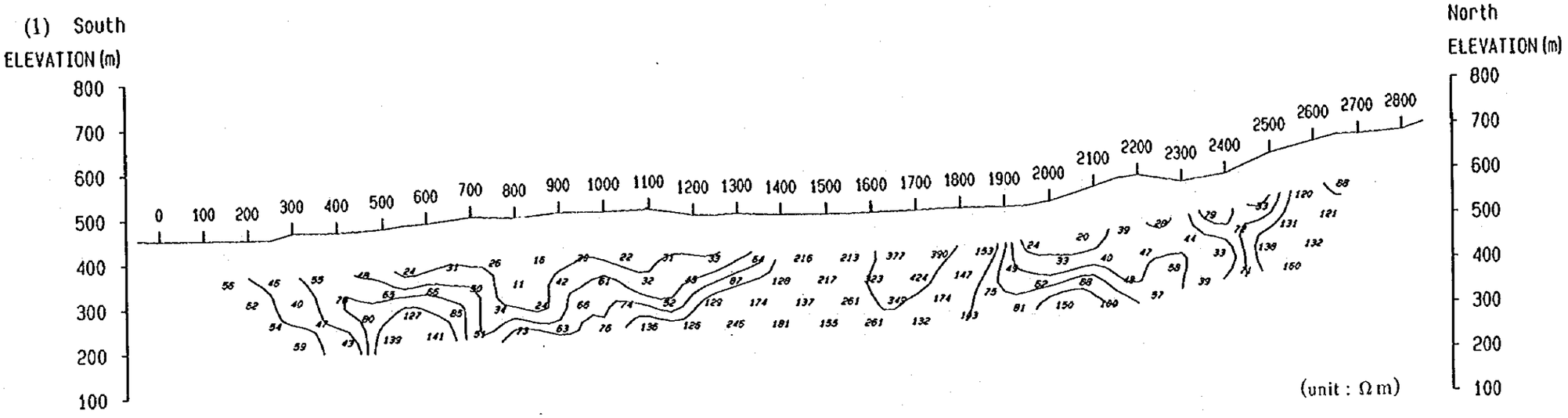

(2) South

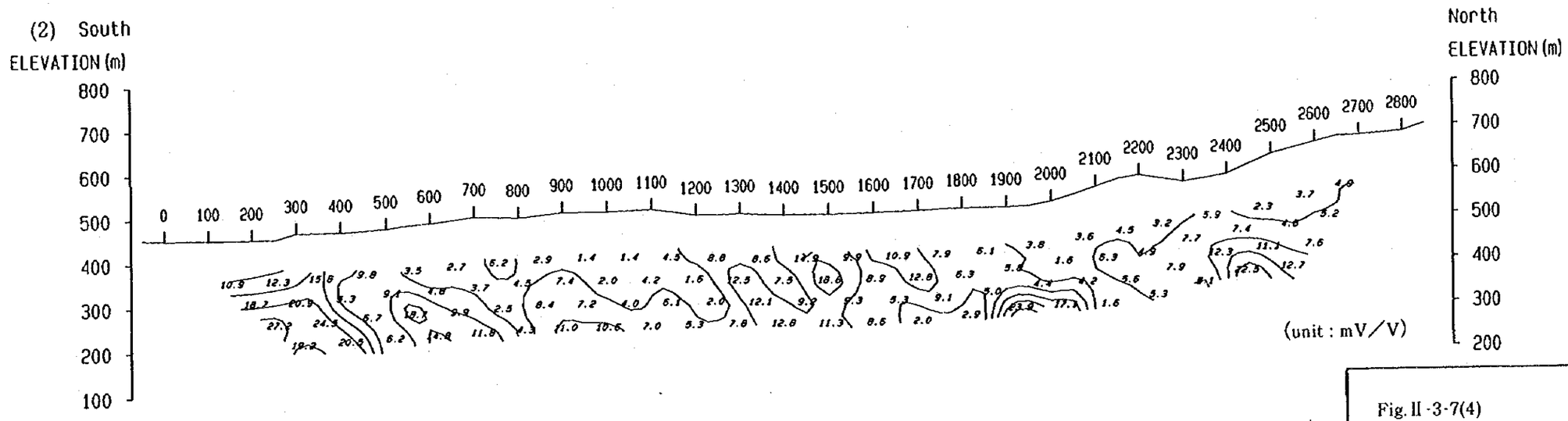

100 0 100 200 300 (m)

Fig. II-3-7(4)

Pseudosection of apparent resistivity(1) and chargeability(2) for profile Ⅳ

(1 : 10,000)

Geophysical Survey (IP), Phase II

Progreso Project, JICA/MMAJ-ENAMI

(1) WEST

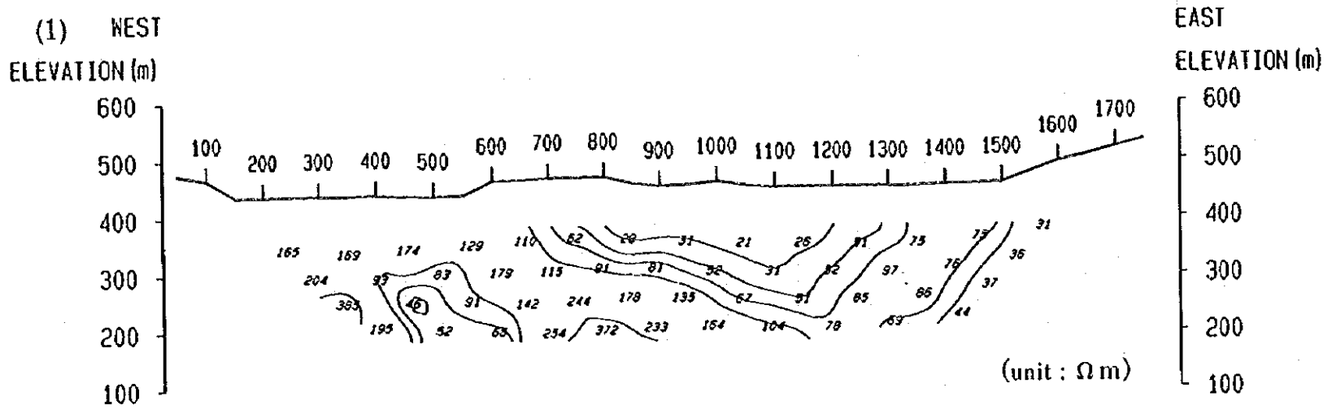

EAST

(2) WEST

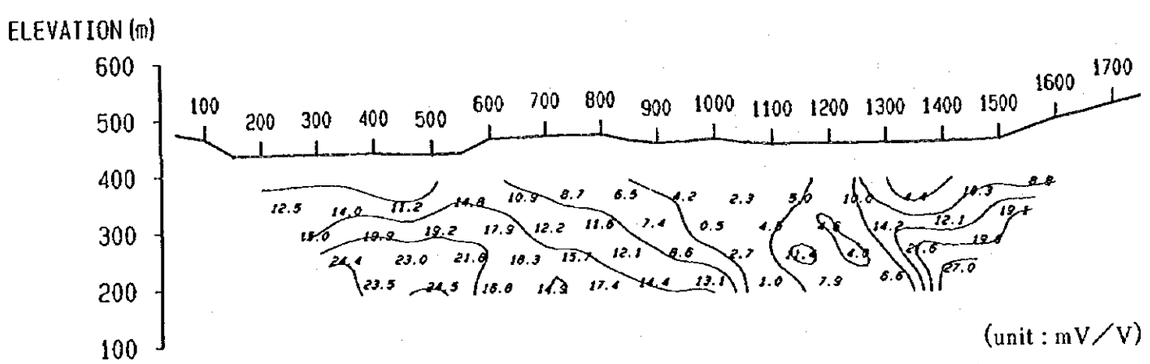

EAST

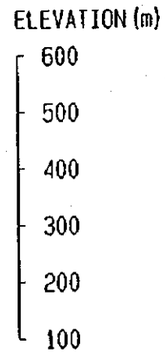

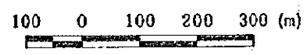

Fig. II-3-7(5)

Pseudosection of apparent resistivity(1) and chargeability(2) for profile V

(1 : 10,000)

Geophysical Survey (IP), Phase II

Progreso Project, JICA/MMAJ-ENAMI

higher from the west of the profile (approx. 5mV/V) to the east (approx. 15mV/V). Local high chargeability (approx. 67mV/V) is seen in the deep zone at measurement point 500, but it is thought to be interference due to some kind of artificial signal.

Profile II (Fig.II-3-7(2))

Taking measurement point 1200 as the boundary, low apparent resistivity is distributed in the south (approx. 10-30Ωm) and high resistivity in the north (approx. 100-250 Ωm). Chargeability is high (approx. 20-60mV/V) to the north of measurement point 1200 and low (approx. 1-20mV/V) to the south.

Profile III (Fig.II-3-7(3))

From the southern tip of the profile, low apparent resistivity (approx. 30-100Ωm) is distributed at measurement point 700, medium apparent resistivity from measurement point 700 to measurement point 1000, and high apparent resistivity (approx. 500-1200Ωm) north of measurement point 1000. Chargeability is high (approx. 30-50mV/V) in the middle of the profile (measurement point 900 to measurement point 1300), medium (approx. 20-40mV/V) north of measurement point 1300, and low (approx. 2-20mV/V) south of measurement point 900.

Profile IV (Fig.II-3-7(4))

Apparent resistivity from measurement point 1400 to 1900 and north of 2500 is high (approx. 100-400 Ωm), while south of measurement point 1400 and from measurement point 1900 to 2500 it is low (approx. 10-100Ωm). Chargeability is low overall and slightly high (approx. 10-20mV/V) in the deep zone from measurement point 1900 to 2500.

Profile V (Fig.II-3-7(5))

Apparent resistivity is low overall (approx. 20-300Ωm), and a low apparent resistivity zone is seen in the shallow zone from measurement point 700 to 1200. Chargeability is rather high (approx. 15-25mV/V) west of measurement point 500 and east of measurement point 1300, and low (below approx. 1-15mV/V) from measurement point 500 to 1300.

3. Laboratory Measurements

The resistivity and chargeability values of core sample measured to get a correlation between the values of measurements on the surface of the earth and the actual values of the rocks below the ground. 30 samples were taken from 3 boring cores dug last year.

The resistivity values of the core samples are distributed in the range of 69.1 - 6770Ωm, by continuously measuring inside the borehole 4.1m (average 6781.6Ωm). Chargeability is in the range of 0.4 - 9.3 (average 3.16). As shown in Fig.II-3-8(1), there is a tendency at each hole for the resistivity value to become higher as the depth increases. Also, as shown in Fig.II-3-8(2), the resistivity values of samples where the chargeability is 3.0 or over are 191.7 - 67704.1Ωm (average11,223.0Ωm), and in samples where the chargeability is 4.0 or over the average is 13196.7 m, and in samples where the chargeability is

5.0 or over the average is 18273.9Ωm. So samples with high chargeability tend to show a higher than average resistivity. Nevertheless, as none of the three boreholes reaches the mineral deposit, the conclusion cannot immediately be drawn from these results that the deposit shows high resistivity-high chargeability. In other words, the deposit itself is high resistivity-high chargeability, but it can also be assumed that the surrounding area is high resistivity-high chargeability.

The measurement results are shown in the Table of Laboratory Measurements in Table II-3-4.

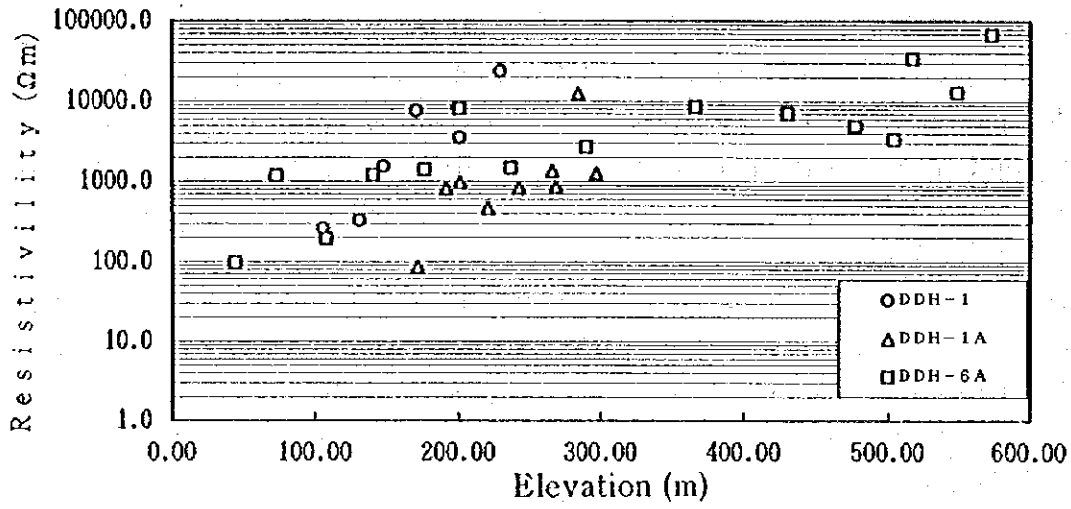

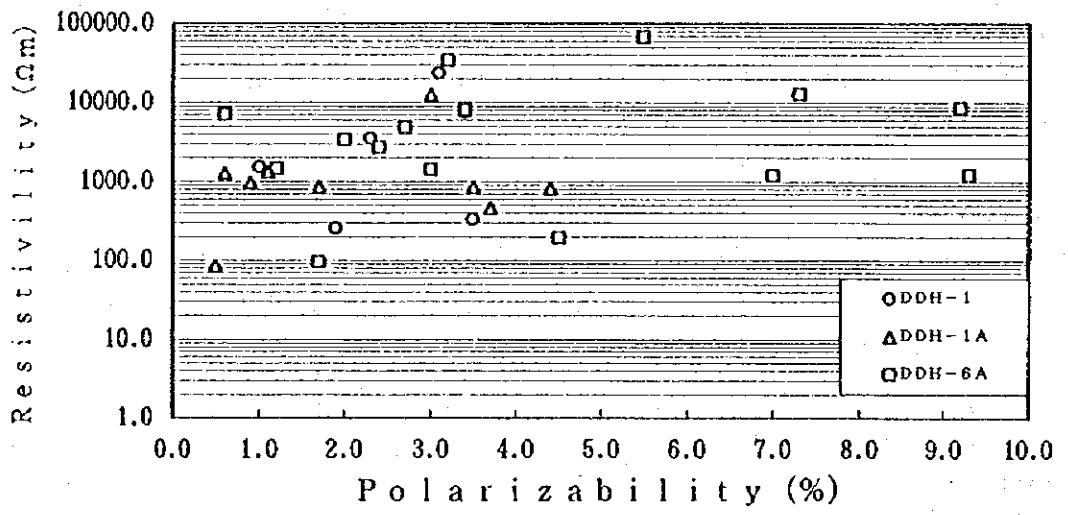

Table II-3-4 Resistivity and chargeability of rock samples

Sample No.	Well name	depth (m)	resistivity (Ω·m)	charge-ability	Description
1	DDH-1	105.8	253.2	1.9	granodiorite, weakly limonitized
2	DDH-1	131.0	324.2	3.5	granodiorite, weakly limonitized
3	DDH-1	147.5	1516.2	1.0	granodiorite
4	DDH-1	170.2	7500.6	3.4	granodiorite
5	DDH-1	201.0	3482.9	2.3	granodiorite py diss.
6	DDH-1	229.5	23435.6	3.1	granodiorite
7	DDH-1A	171.0	84.4	0.5	conglomerate
8	DDH-1A	191.6	815.7	4.4	dacitic volcanics py diss.
9	DDH-1A	200.8	964.8	0.9	dacitic volcanics py rare
10	DDH-1A	220.5	462.4	3.7	dacitic volcanics py film
11	DDH-1A	242.2	833.3	3.5	dacitic volcanics py film
12	DDH-1A	265.8	1342.7	1.1	dacitic volcanics py rare
13	DDH-1A	268.0	851.5	1.7	dacitic volcanics py none
14	DDH-1A	284.0	12556.8	3.0	dacitic volcanics py rare
15	DDH-1A	296.5	1265.7	0.6	dacitic volcanics py rare
16	DDH-6A	44.0	95.7	1.7	conglomerate
17	DDH-6A	72.5	1181.1	7.0	calcite rich
18	DDH-6A	107.8	191.7	4.5	siliceous limestone
19	DDH-6A	140.0	1196.4	9.3	siliceous limestone
20	DDH-6A	176.0	1402.5	3.0	sandstone
21	DDH-6A	200.5	7981.7	3.4	siliceous limestone
22	DDH-6A	236.5	1458.3	1.2	siliceous limestone
23	DDH-6A	289.5	2680.0	2.4	siliceous limestone
24	DDH-6A	365.9	8471.9	9.2	siliceous limestone
25	DDH-6A	430.0	7028.5	0.6	siliceous limestone
26	DDH-6A	477.0	4859.0	2.7	tuffaceous sandstone py diss.
27	DDH-6A	504.0	3375.2	2.0	andesitic volcanics py-cp diss.
28	DDH-6A	517.6	34026.7	3.2	andesitic volcanics py diss.
29	DDH-6A	549.0	12816.2	7.3	andesitic volcanics py rare
30	DDH-6A	573.0	67704.1	5.5	andesitic volcanics py none

4. PEM Mode Measurement Results

With the PEM method, in general when the resistivity in the vicinity of the borehole is lower than the resistivity of the surrounding strata, such as mineral deposits, a secondary magnetic field is produced, centering on subterranean low resistivity, due to the influence of signals (primary magnetic field).

Figs.II-3-9(1) - (5) show the results of measuring the Z component by the PEM method in DDH-1A. Normally, when a low resistivity zone, such as mineral deposits, exists in the vicinity of the borehole, marked changes in measurement values due to the influence of the deposit can be seen, but with the results of measurements taken using every transmmiter loop, no clear changes in the measurement values are seen. Nevertheless, all 5 types of measurement results show positive convex changes which peak at around a depth of 140m. From this it is assumed that the boundary between the surface layer and the layer below is around a depth of 140m. In fact, judging from the boring results, this corresponds to the fact that alluvium is distributed from the surface to a depth of 142.0m and below 142.0m volcanic sedimentary rock is distributed.

3-3-2 Interpretation Results

As explained in 3-3-1, the AMT and IP measurement data include topographical effects and various other elements apart from the subterranean resistivity structure. In particular, static and topographical effects were seen to a large extent in the survey area when the AMT method was used. Nevertheless, by conducting two-dimensional joint inversion interpretation using both the IP method and the AMT method at the same time, it was possible to carry out interpretation from the shallow zone to the deep zone excluding these effects. The results of two-dimensional inversion interpretation by IP and AMT independently for each profile are explained below, including the improvements made by two-dimensional joint inversion interpretation.

Profile I

From the IP interpretation section shown in Fig.II-3-10(1), resistivity of around 100-250 Ωm is distributed in stratified form from the surface to alt. 300m, with the resistivity gradually becoming lower from alt. 300m. Judging from the fact that the resistivity values gradually become higher below alt. 200m according to the AMT interpretation section in Fig.II-3-11, the depth of investigation by the IP method is not thought to extend as far as the high resistivity zone. Conversely, from the IP interpretation results, a resistivity layer of approx. 200 Ωm is distributed from the surface to a depth of 50m and a resistivity layer of approx. 100 Ωm is distributed below that to a depth of 100m, but only a resistivity layer of approx. 100 Ωm from the surface to a depth of 60m was analyzed by the AMT method, and the detailed resistivity structure of the shallow zone which could not be obtained by the AMT method was obtained using the IP method. With the exception of such detailed zones, virtually the same results up to alt. 200m were obtained by the AMT and

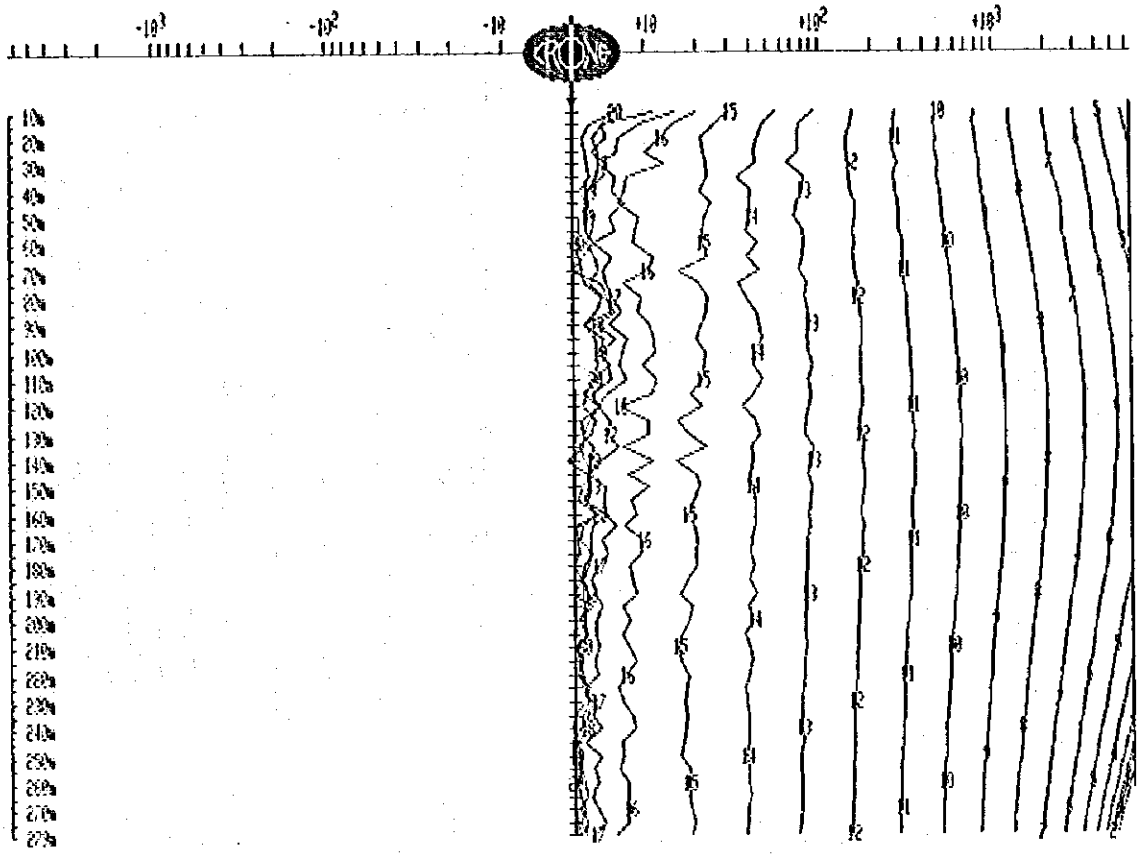

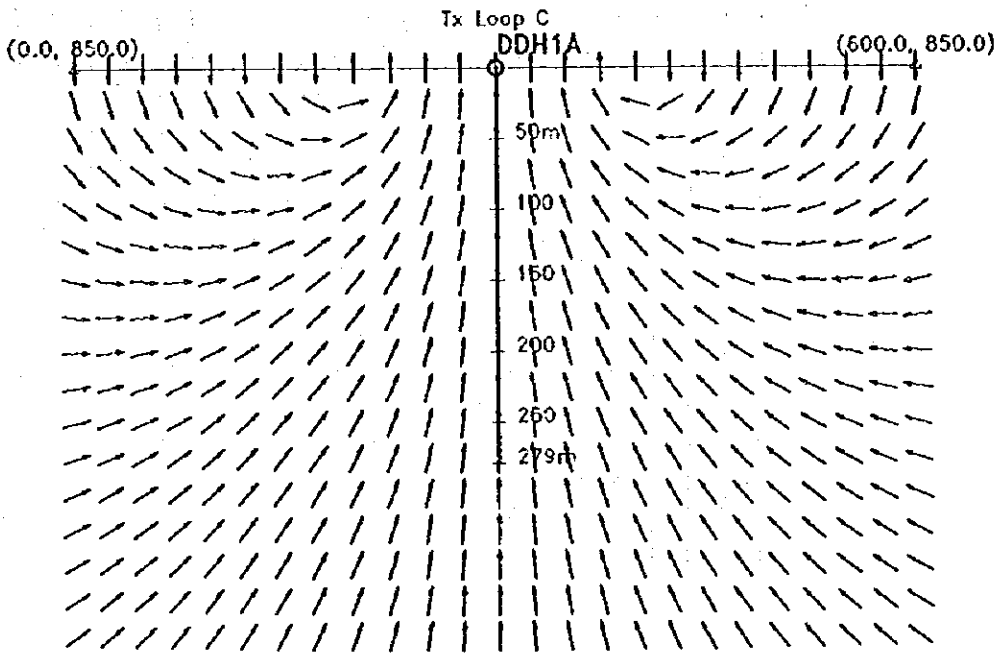

Fig. II-3-9(1)

Pulse EM response and interpretation from central loop for DDH-1A

Geophysical Survey (PEM), Phase II

Progreso Project, JICA/MMAJ-ENAMI

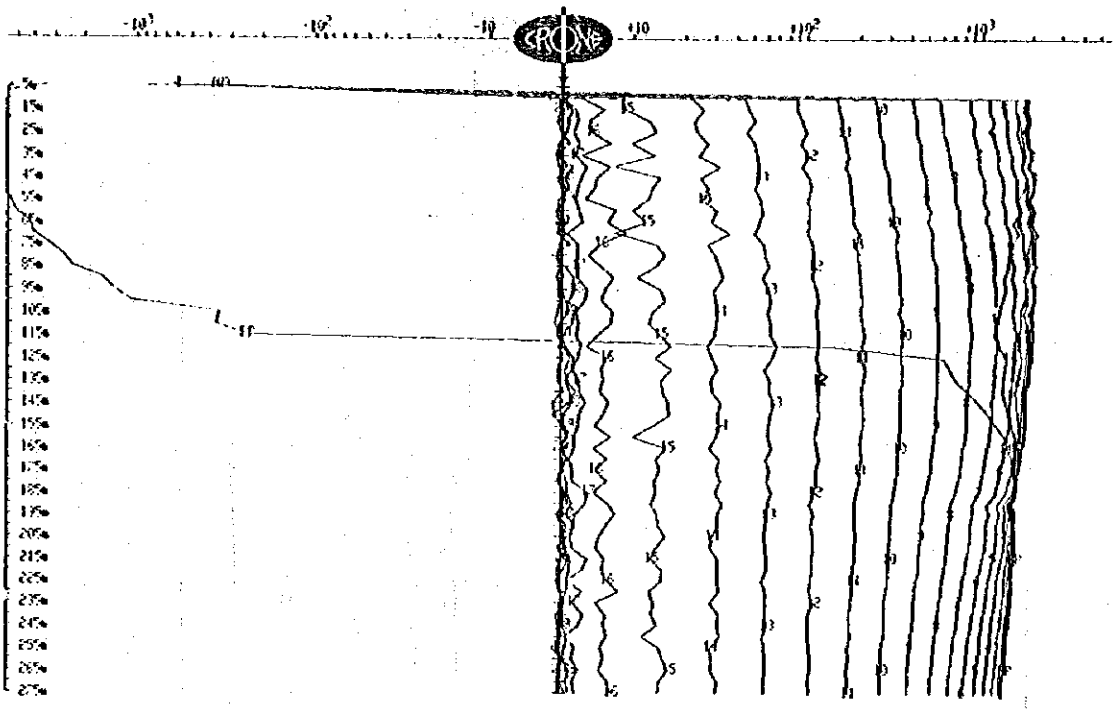

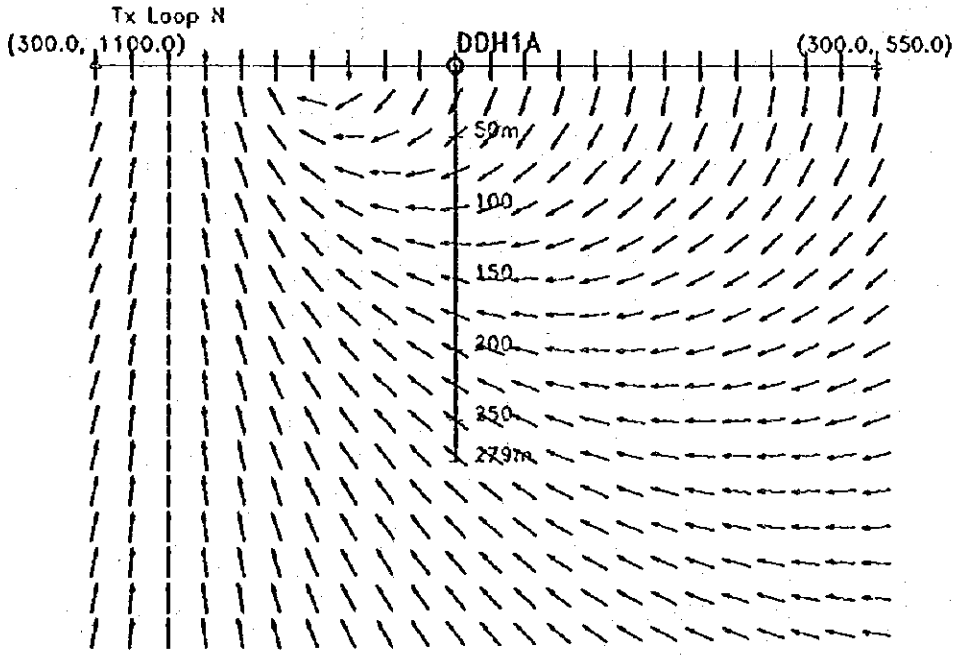

Fig. II-3-9(2)

Pulse EM response and interpretation from north loop for DDH-1A

Geophysical Survey (PEM), Phase II

Progreso Project, JICA/MMAJ-ENAMI

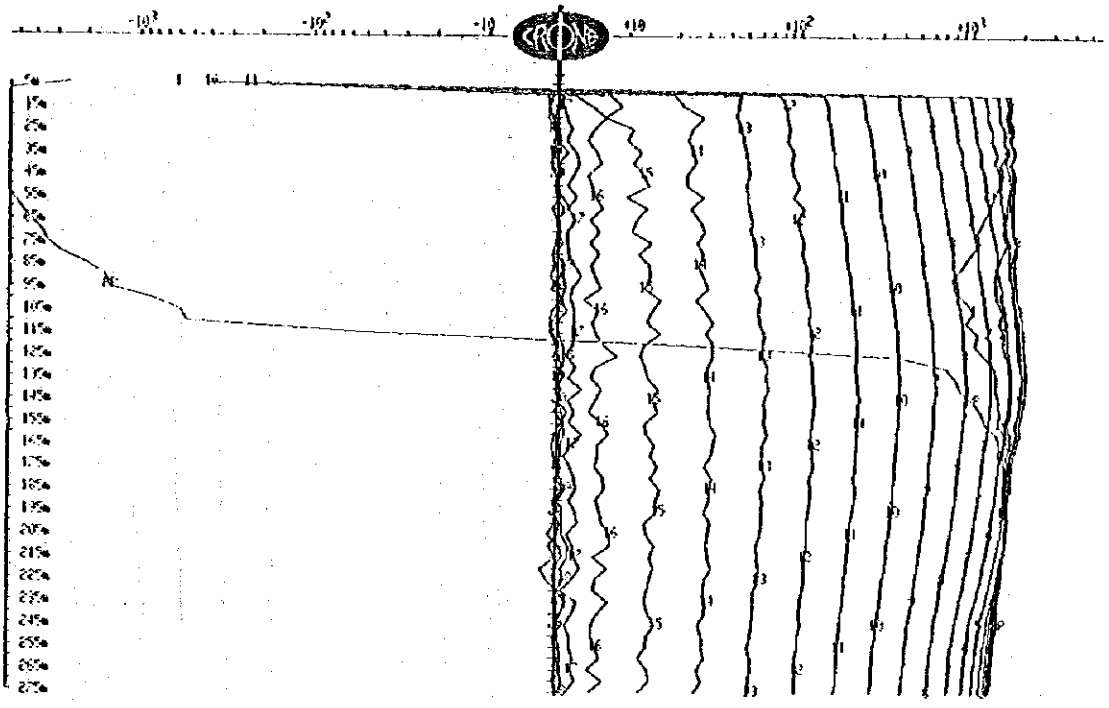

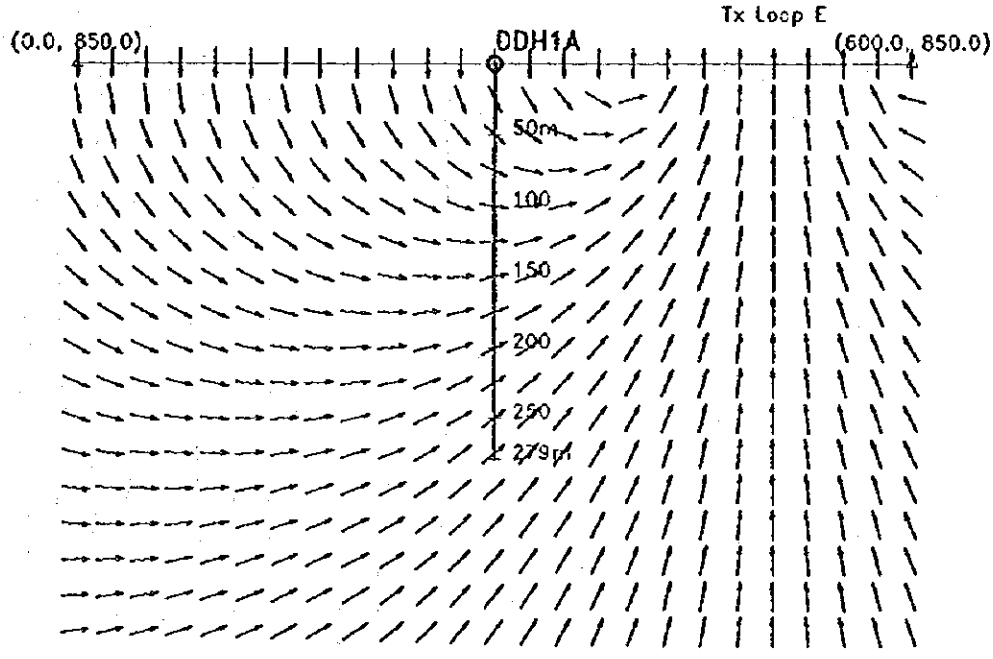

Fig. II-3-9(3)

Pulse EM response and interpretation from east loop for DDH-1A

Geophysical Survey (PEM), Phase II

Progreso Project, JICA/MMAJ-ENAMI

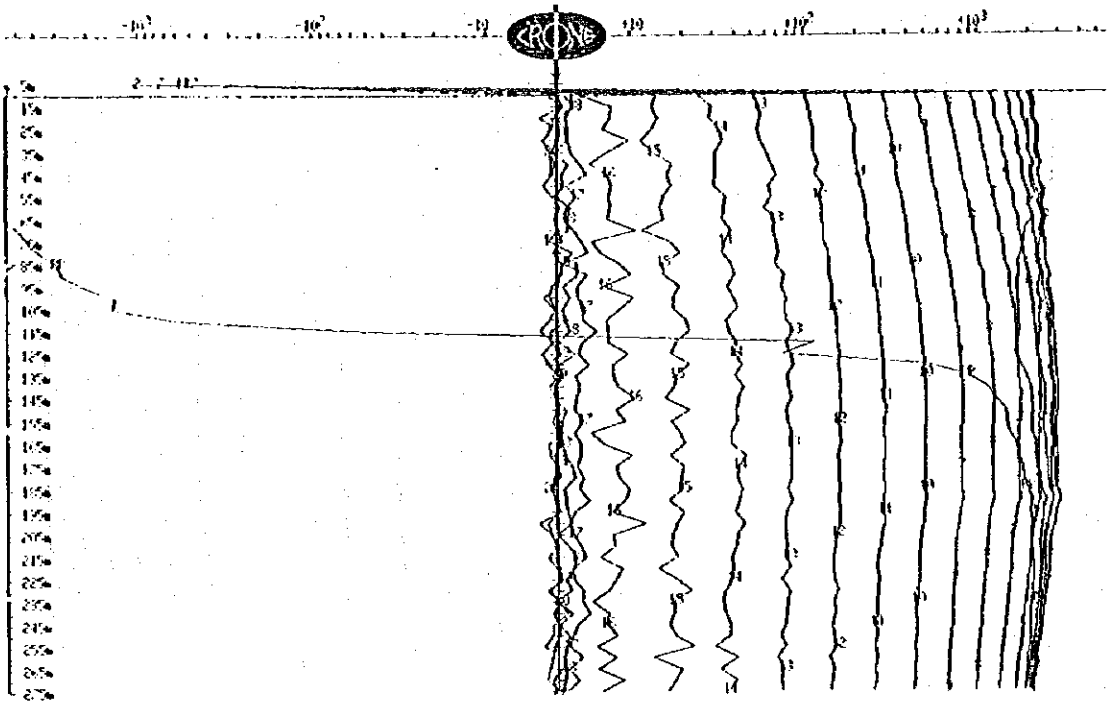

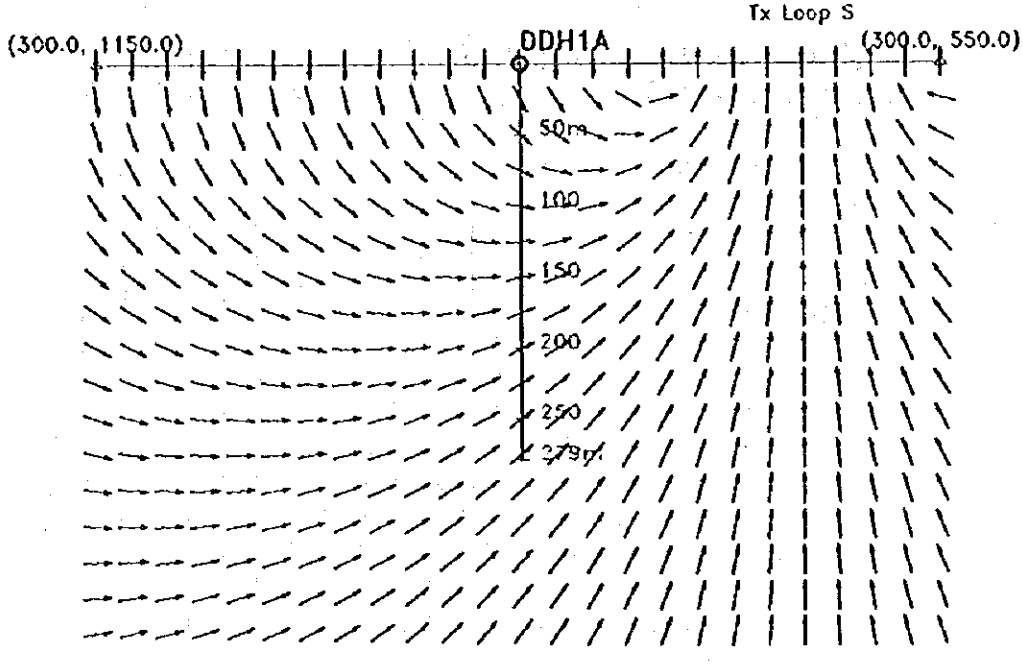

Fig. II-3-9(4)

Pulse EM response and interpretation from south loop for DDH-1A

Geophysical Survey (PEM), Phase II

Progreso Project, JICA/MMAJ-ENAMI

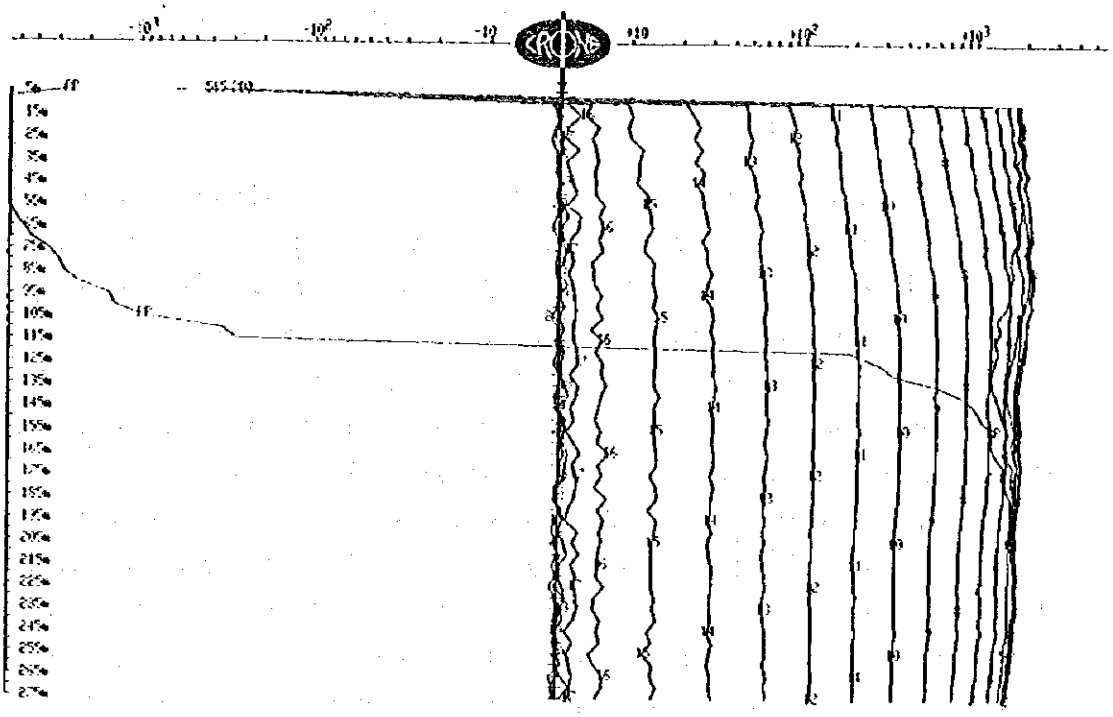

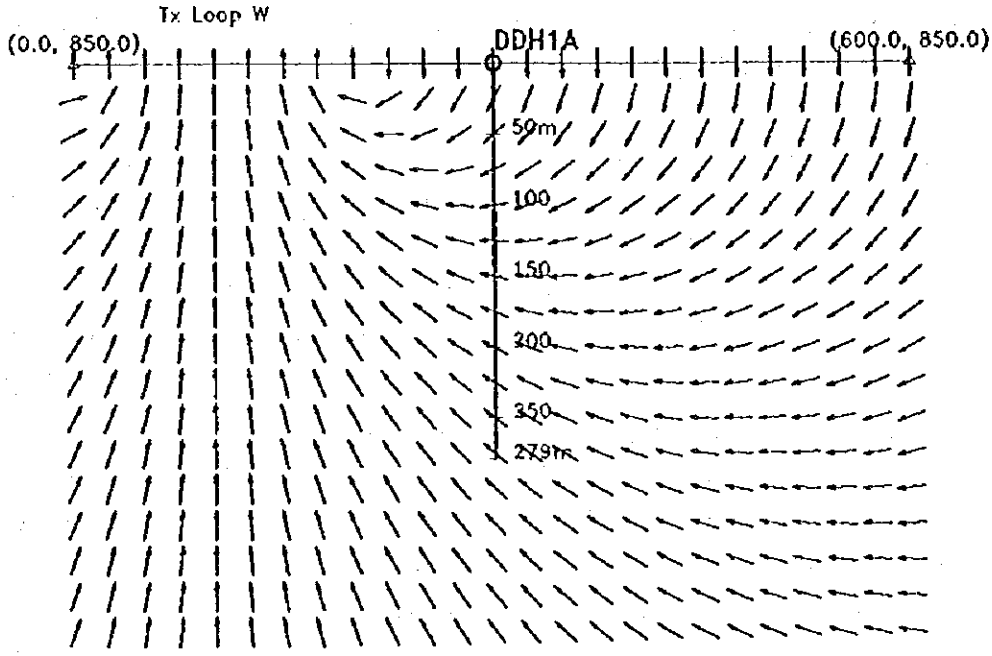

Fig. II-3-9(5)

Pulse EM response and interpretation from west loop for DDH-1A

Geophysical Survey (PEM), Phase II

Progreso Project, JICA/MMAJ-ENAMI

IP methods, and below the IP survey depth of alt. 200m, a high resistivity layer again rose especially at measurement points 400 and 600. According to the joint inversion results in Fig.II-3-12(1), making full use of the information on the shallow zone by the IP method and the information on the deep zone by the AMT method, a resistivity layer of approx. 200Ωm is distributed up to 50m below the surface, a stratified structure of approx. 100Ωm is distributed from 100m-200m, with a low resistivity layer of approx. 60-70 Ωm below that. A resistivity layer of over 100Ωm is again distributed virtually horizontally from around alt. 100m, and the resistivity layer gradually becomes higher the deeper it goes.

With regard to chargeability, when the results obtained by independent IP interpretation (Fig.II-3-10(2)) and those obtained by joint inversion (Fig.II-3-12(2)) are compared, whereas in the case of the former a distribution zone of over 30mV/V extends from alt. 200m to the deep zone, in the case of the latter the zone closes at alt. 100m. This is thought to be because the depth of investigation does not reach below alt. 200m by independent IP method, as seen in the resistivity structure. Similarly, from the results of interpretation by independent IP method, the fact that the distribution zone extends east from measurement point 800 is thought to be because little information was obtained on either end of the profile using only the dipole-dipole method, making the interpretation less accurate.

Profile II

Looking at the resistivity structure from the surface to alt. 300m according to the IP interpretation section shown in Fig.II-3-13(1), a low resistivity layer of approx. 10Ωm - 80Ωm is distributed south of measurement point 1200, a resistivity layer of approx. 100Ωm - 200Ωm is distributed north of measurement point 1200 to measurement point 1900, and a resistivity layer of below 100Ωm is again distributed north of measurement point 1900. Looking at the resistivity structure below alt. 300m according to the AMT interpretation section in Fig.II-3-14, taking measurement point 1300 as the boundary, relatively high resistivity of over 300Ωm is distributed to the south, and resistivity of below 300Ωm is distributed to the north of measurement point 1300. Observing the high resistivity of over 700Ωm south of the profile, the intrusive rock peaks at measurement point 800 according to the results of AMT interpretation. But according to the results of joint inversion interpretation in Fig.II-3-15(1), virtually homogeneous rock of over 1000Ωm is distributed below alt. 200m. This is thought to be because, according to independent AMT interpretation, a thin low resistivity layer in the shallow zone from measurement point 200 to measurement point 800 affected the interpretation of the deep zone, but a better interpretation of the low resistivity layer in the shallow zone was obtained by joint inversion and the structure of the shallow zone was analyzed meaningfully, and as a result the deep zone was not affected by the influence of the shallow zone. Moreover, using joint inversion interpretation at the northern end of the profile, distribution of low resistivity which was seen in the results of the IP interpretation is apparent.

With regard to chargeability by the IP method alone (Fig.II-3-13(2)), a chargeability zone of over

30mV/V is broadly distributed south of measurement point 600, and a chargeability zone of over 50mV/V is broadly distributed south of measurement point 1100. According to the results of joint inversion interpretation (Fig.II-3-15(2)), the distribution zone of chargeability over 30mV/V is found south of measurement point 1000, and distribution zones of chargeability over 50mV/V are found in two places, from measurement point 1100 to measurement point 1500, and south of measurement point 1800. Distribution was analyzed up to alt. 200m.

Profile III

Looking at the structure of the surface zone according to the resistivity structure section by IP method shown in Fig.II-3-16(1), a resistivity zone of over 500Ωm is distributed to the north of measurement point 1000 and a resistivity zone of for the most part less than 100 m is distributed to the south of measurement point 900. In particular, a low resistivity zone of around 50Ωm is distributed in the shallow zone from measurement point 300 to measurement point 500. According to the results of AMT interpretation (Fig.II-3-17), a resistivity zone of less than 50Ωm is distributed in the surface zone from measurement point 200 to measurement point 400, in the same way as the IP results, and a resistivity zone of less than 50 Ωm is also seen from measurement point 600 to measurement point 1000. From the results of IP interpretation, it is assumed that measurement point 900 is a rather low resistivity layer of under 100Ωm, but this differs to the results obtained by AMT interpretation. The topography of this profile is extremely steep and the topographic effects cannot be reproduced entirely by modeling, and it is thought that this is the reason why rather different results were obtained by the IP method and the AMT method. As for the structure below a depth of 200m, according to the results of AMT interpretation alone, to the south of the profile a resistivity zone of under 300Ωm is distributed in the deep zone, and to the north of the profile a resistivity zone of over 300Ωm rises steeply up to the surface zone in the form of an anomaly. This is also assumed to be due to the influence of the shallow zone south of the profile. According to the results of joint inversion interpretation shown in Fig.II-3-18(1), excluding the influence of the low resistivity anomaly in the shallow zone, the topographical effects, etc., a resistivity layer of less than 200Ωm in the shallow zone from measurement point 100 to measurement point 1000 is thickly distributed up to a depth of around 300m in the vicinity of measurement point 400, and to the north of measurement point 1100 a resistivity zone of over 500Ωm is distributed up to the shallow zone.

Chargeability distribution of over 50mV/V, apparent over a broad area north of measurement point 800 in the chargeability interpretation section by IP method alone shown in Fig.II-3-16(2), is seen to be an anomaly zone concentrated from measurement point 900 to measurement point 1200 according to the results of joint inversion shown in Fig.II-3-18(2).

Profile IV

The IP resistivity interpretation section is shown in Fig.II-3-19(1). To the south of measurement point 1300 and to the north of measurement point 1900 a resistivity layer of under 100Ωm is distributed in the surface zone, and from measurement point 1400 to measurement point 1800 a resistivity zone with an anomaly of 100Ωm is seen in the surface zone. In the AMT interpretation resistivity section shown in Fig.II-3-20, resistivity layers of less than 100Ωm are likewise distributed in the surface zone south of measurement point 1300 and north of measurement point 1900. The results correspond to those obtained by IP interpretation. As for the structure of the deep zone, a resistivity zone with an anomaly of 300Ωm is distributed mainly from alt. 100m to -200m at measurement point 600 and extends to measurement point 1700 in the shallow zone. Moreover, a resistivity zone of over 300Ωm is distributed from measurement point 200 to below measurement point 2400. Also, a resistivity zone of less than 100Ωm is distributed from alt. -200m from measurement point 1000 to measurement point 1800. This low resistivity zone is assumed to be a low resistivity anomaly that has become extremely low resistivity because of measurement data matching, as a result of a high resistivity zone of approx. 900Ωm being distributed linking the high resistivity zones south of the profile from alt. 300m to alt. 0m directly above. In fact, from the results of joint inversion interpretation shown in Fig.II-3-21(1), resistivity of over 300Ωm is distributed from alt. 500m to 300m from measurement point 1300 to measurement point 1700, and in the deep zone a resistivity structure of over 100Ωm is distributed. To the south and north of the profile, a high resistivity zone is distributed rising to the shallow zone, and a resistivity layer of less than 100Ωm is distributed in the surface zone south of measurement point 1400 and from measurement point 1900 to 2600.

According to the results of chargeability interpretation by the IP method shown in Fig.II-3-19(2), a distribution zone of over 30mV/V is seen extending down to the southern end of the profile, but using the dipole-dipole method, there is little measurement point density and in fact it is thought to be a small anomaly as shown in Fig.II-3-21(2).

Profile V

The resistivity section obtained by the IP method is shown in Fig.II-3-22(1). In the surface zone, a resistivity layer of less than 100Ωm is distributed to the east of measurement point 700, and a resistivity zone of over 300Ωm rises below alt. 300m from measurement point 700 to 1200. According to the results of AMT interpretation shown in Fig.II-3-23, the resistivity structure of the shallow zone virtually corresponds to the results obtained by the IP method, a resistivity zone of over 300Ωm is seen at the surface at measurement point 200 and is distributed from a depth of 50m to 100m from measurement point 600 to measurement point 1200. It shows a structure which falls to about alt. 300m at measurement point 400, gradually deepening to alt. 200m east of measurement point 1200. Moreover, in the deep zone, a high resistivity anomaly exceeding 10000Ωm is distributed from alt. 0m to around 100m at measurement point

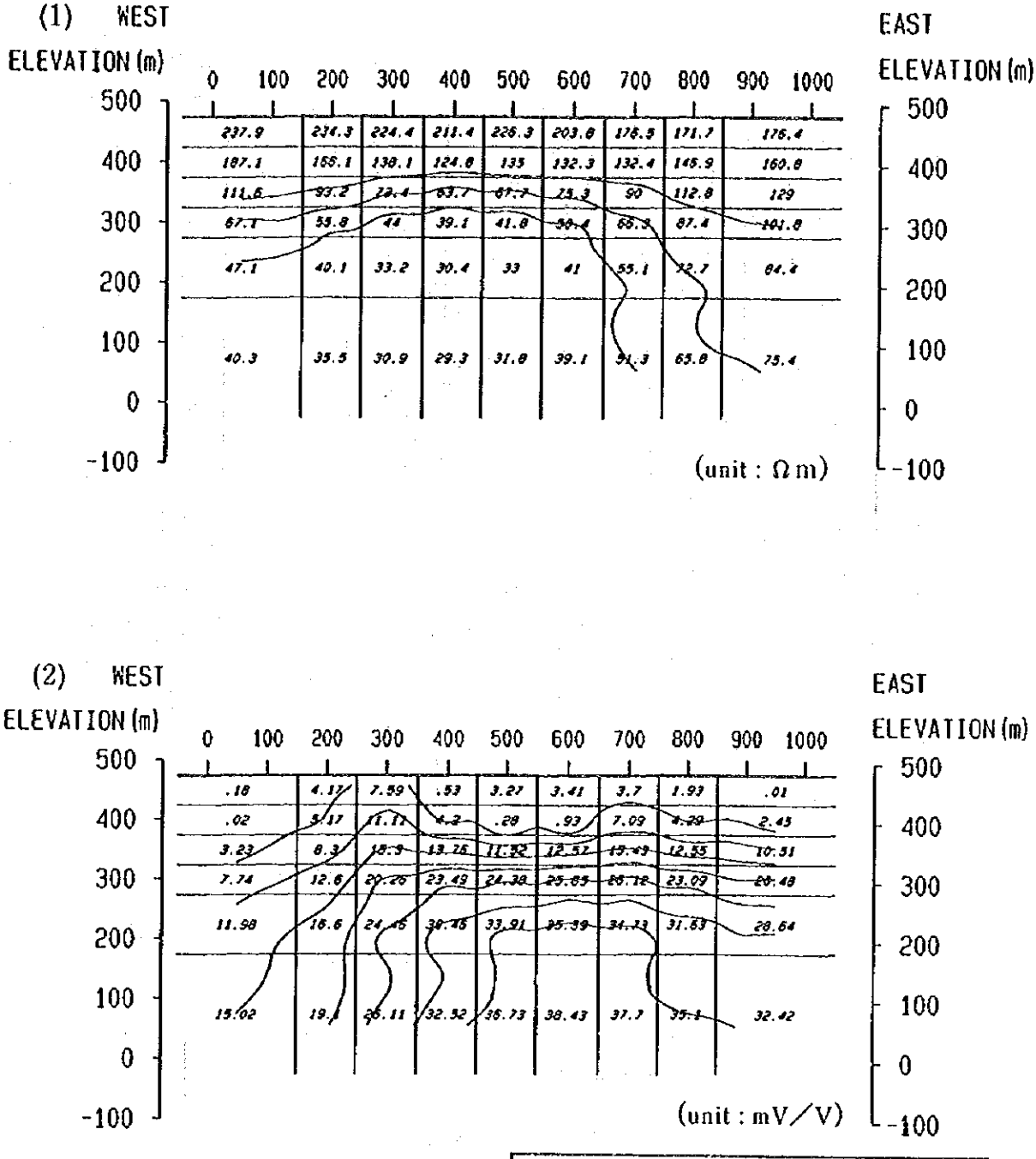

Fig. II-3-10

IP resistivity(1) and chargeability(2) section from 2D inversion result for profile I

(1 : 10,000)

Geophysical Survey (IP), Phase II

Progreso Project, JICA/MMAJ-ENAMI

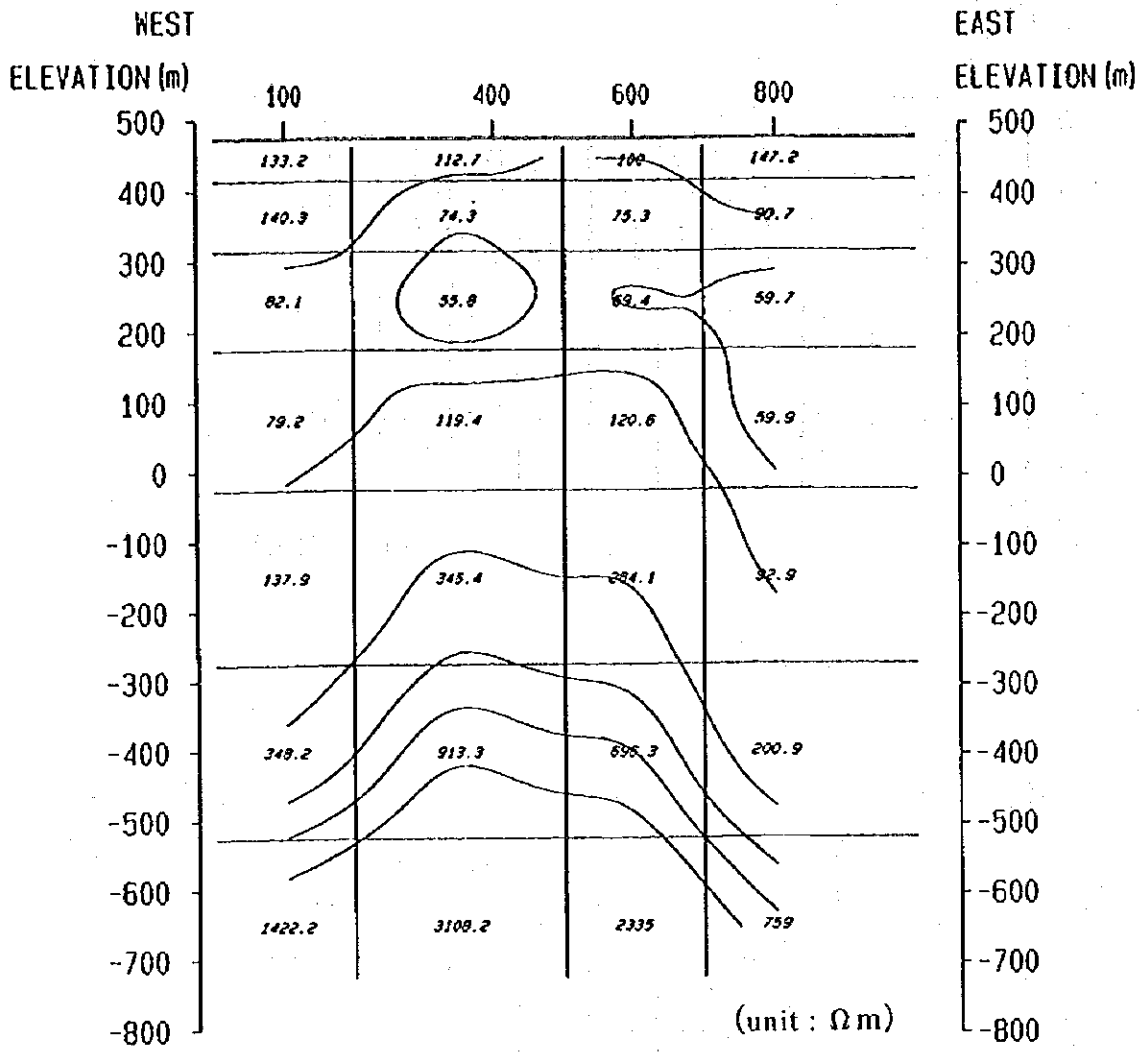

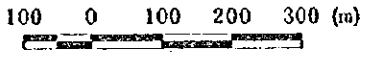

Fig. II-3-11

AMT resistivity section from 2D inversion result for profile I

(1 : 10,000)

Geophysical Survey (AMT), Phase II

Progreso Project, JICA/MMAJ-ENAMI

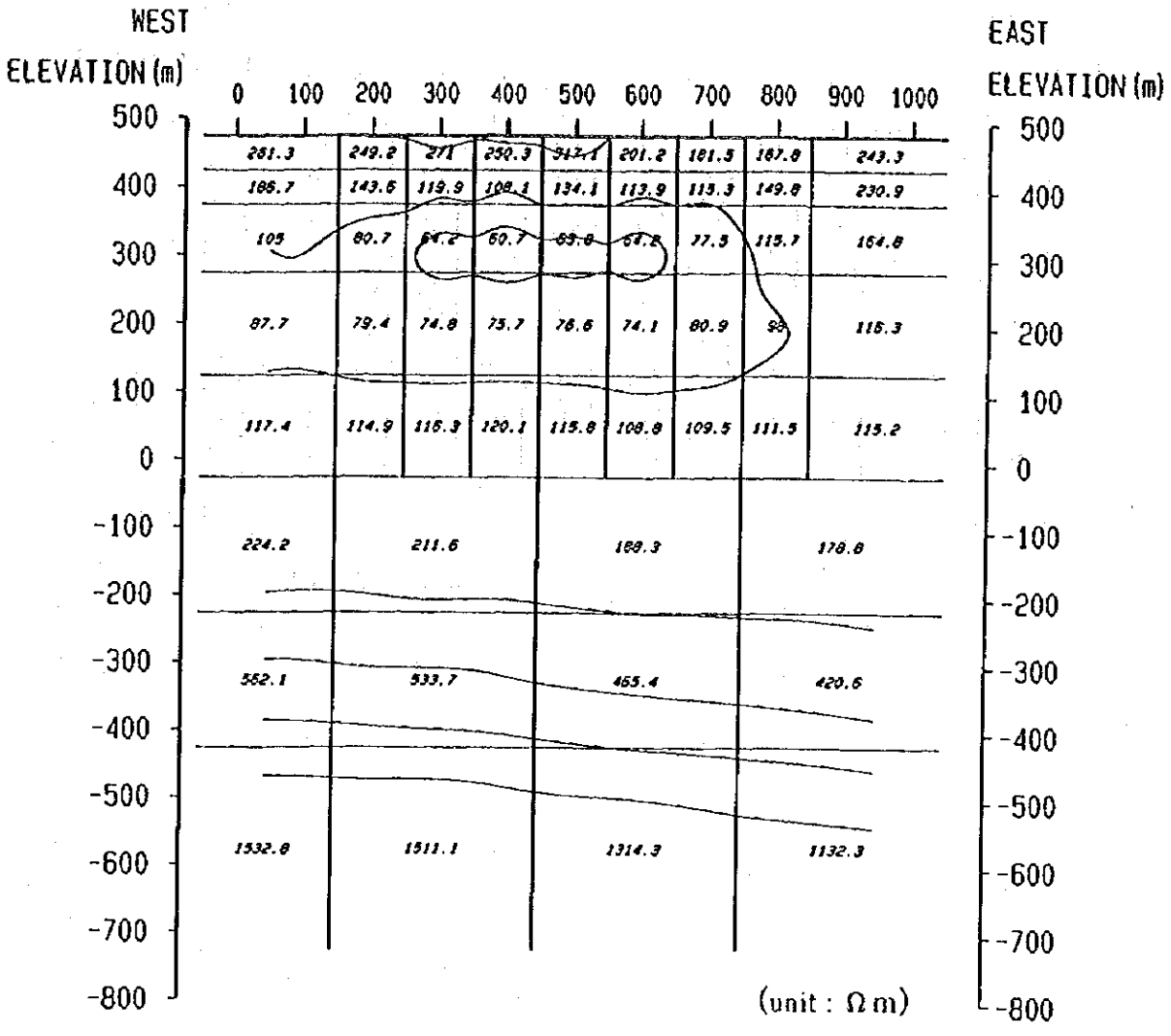

Fig. II-3-12(1)

Resistivity section from 2D joint inversion reslt for profile I

(1 : 10,000)

Geophysical Survey, Phase II

Progreso Project, JICA/MMAJ-ENAMI

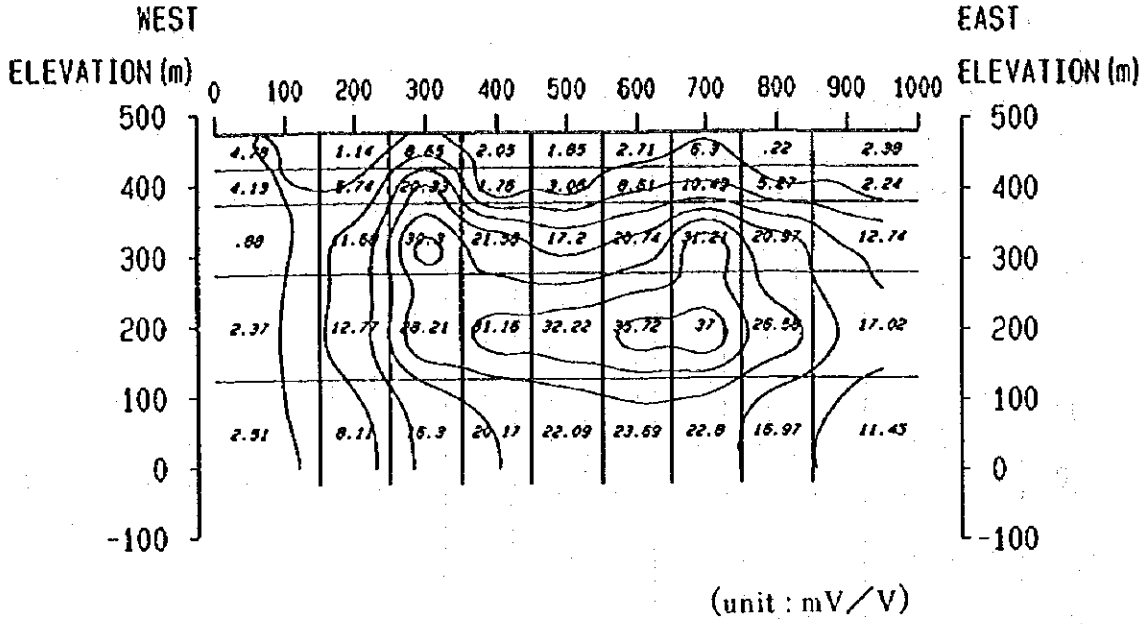

(unit : mV／V)

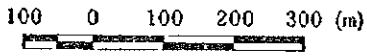

Fig. II -3-12(2)

Chargeability section from 2D joint inversion result for profile I

(1 : 10,000)

Geophysical Survey, Phase II

Progreso Project, JICA/MMAJ-ENAMI

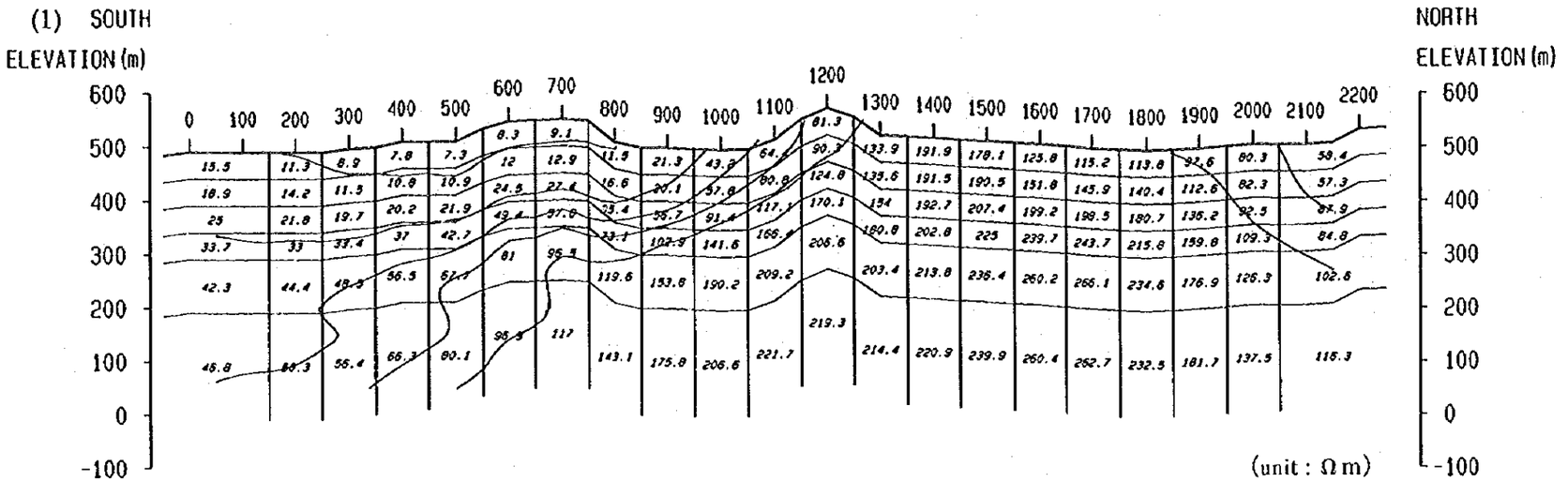

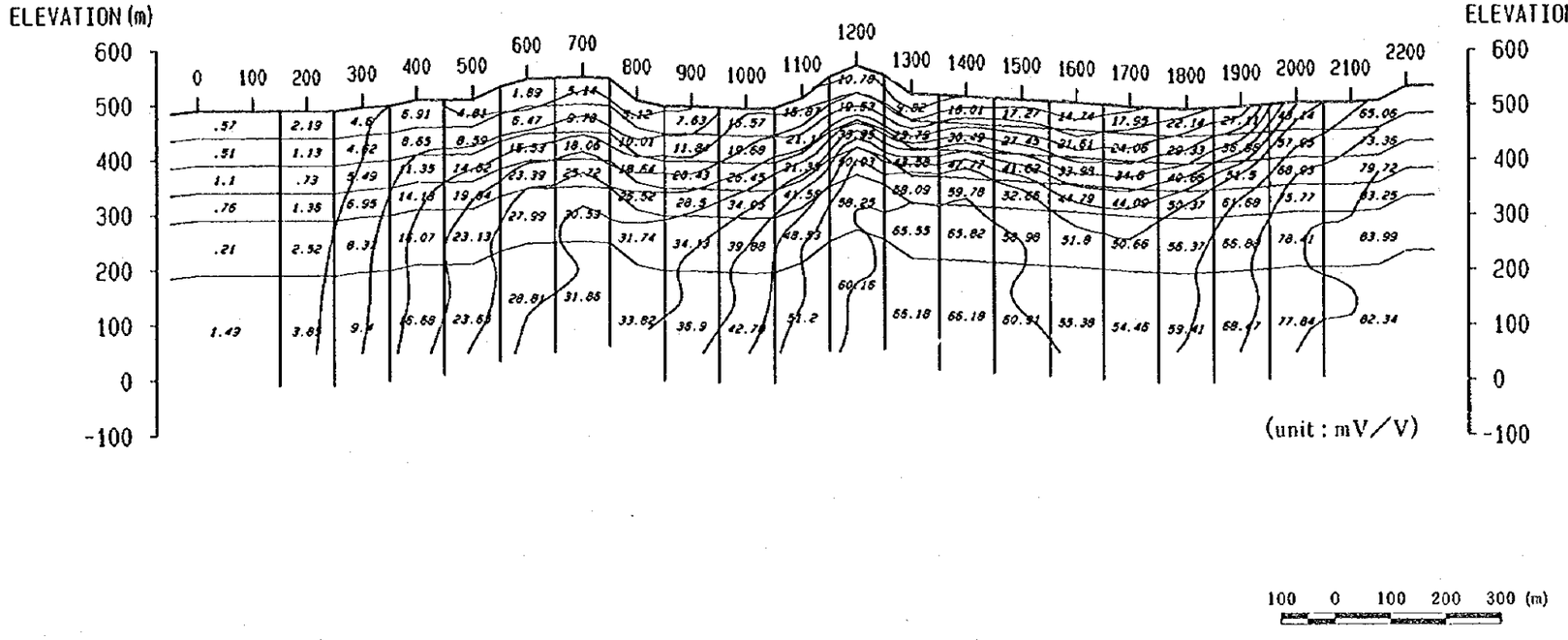

Fig. II-3-13

IP resistivity(1) and chargeability(2) section from 2D inversion result for profile II

(1 : 10,000)

Geophysical Survey (IP), Phase II

Progreso Project, JICA/MMAJ-ENAMI

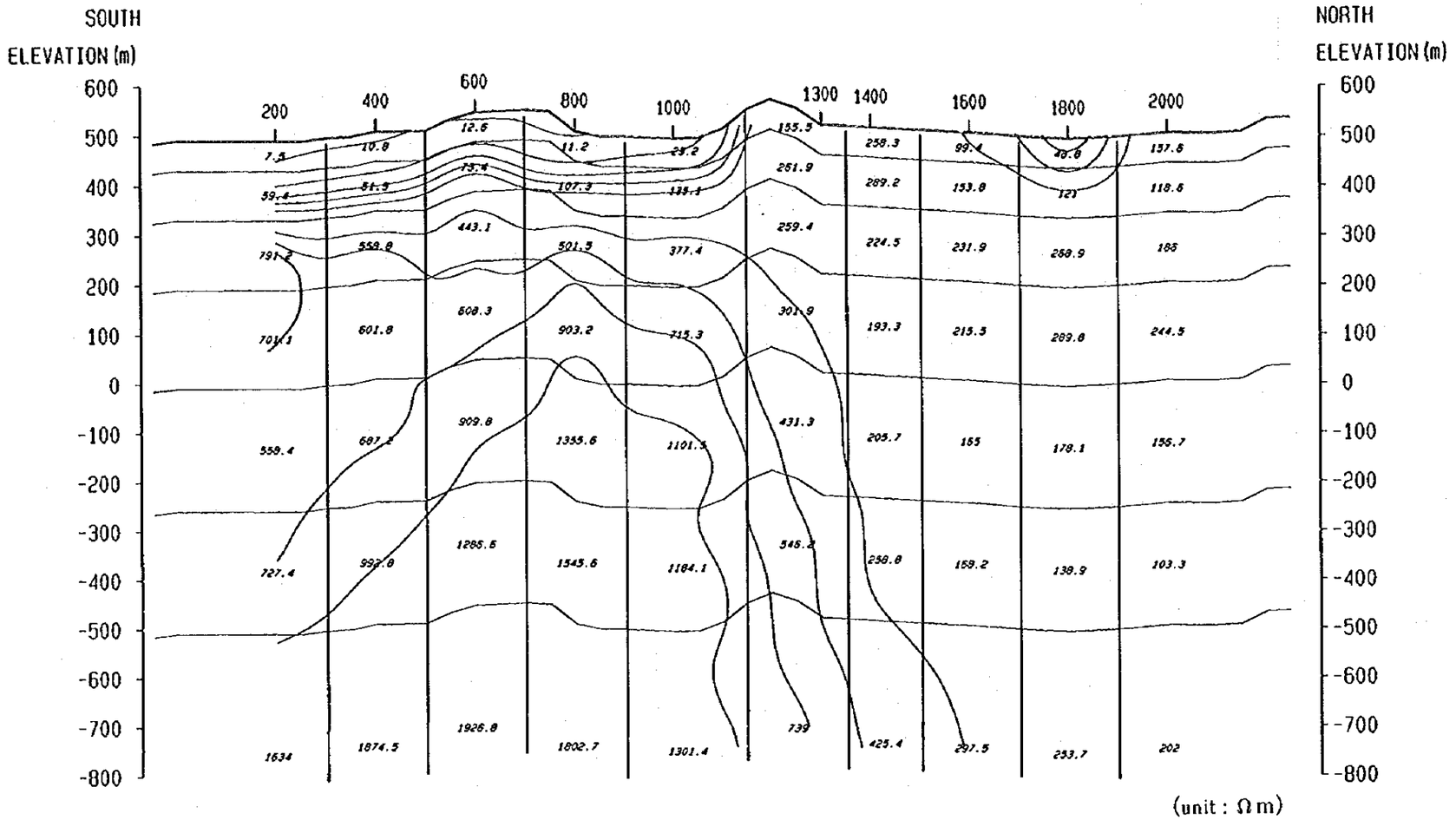

100 0 100 200 300 (m)

Fig. II-3-14

AMT resistivity section from 2D inversion result for profile II

(1 : 10,000)

Geophysical Survey (AMT), Phase II

Progreso Project, JICA/MMAJ-ENAMI

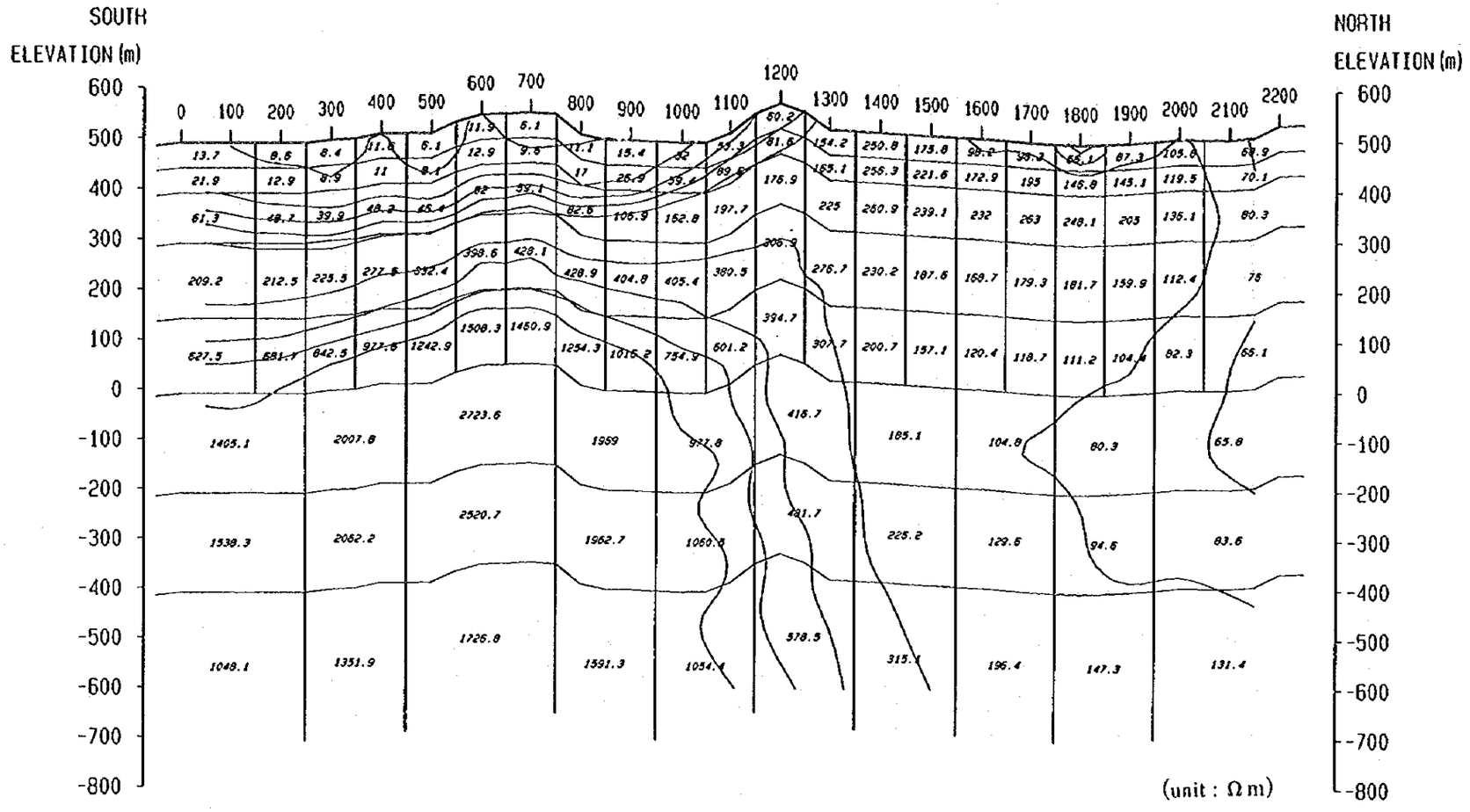

100 0 100 200 300 (m)

Fig. II-3-15(1)

Resistivity section from 2D joint inversion reslt for profile II

(1 : 10,000)

Geophysical Survey, Phase II

Progreso Project, JICA/MMAJ·ENAMI

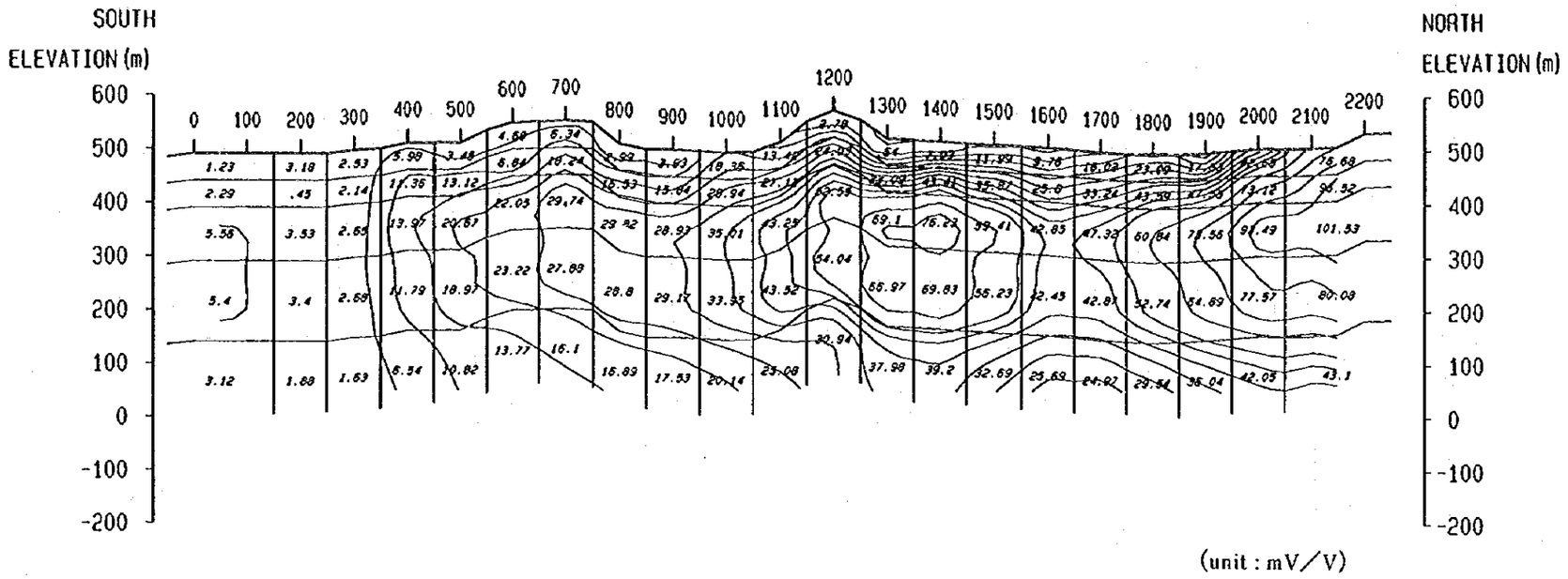

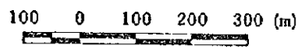

Fig. II-3-15(2)

Chargeability section from 2D joint inversion result for profile II

(1 : 10,000)

Geophysical Survey, Phase II

Progreso Project, JICA/MMAJ-ENAMI

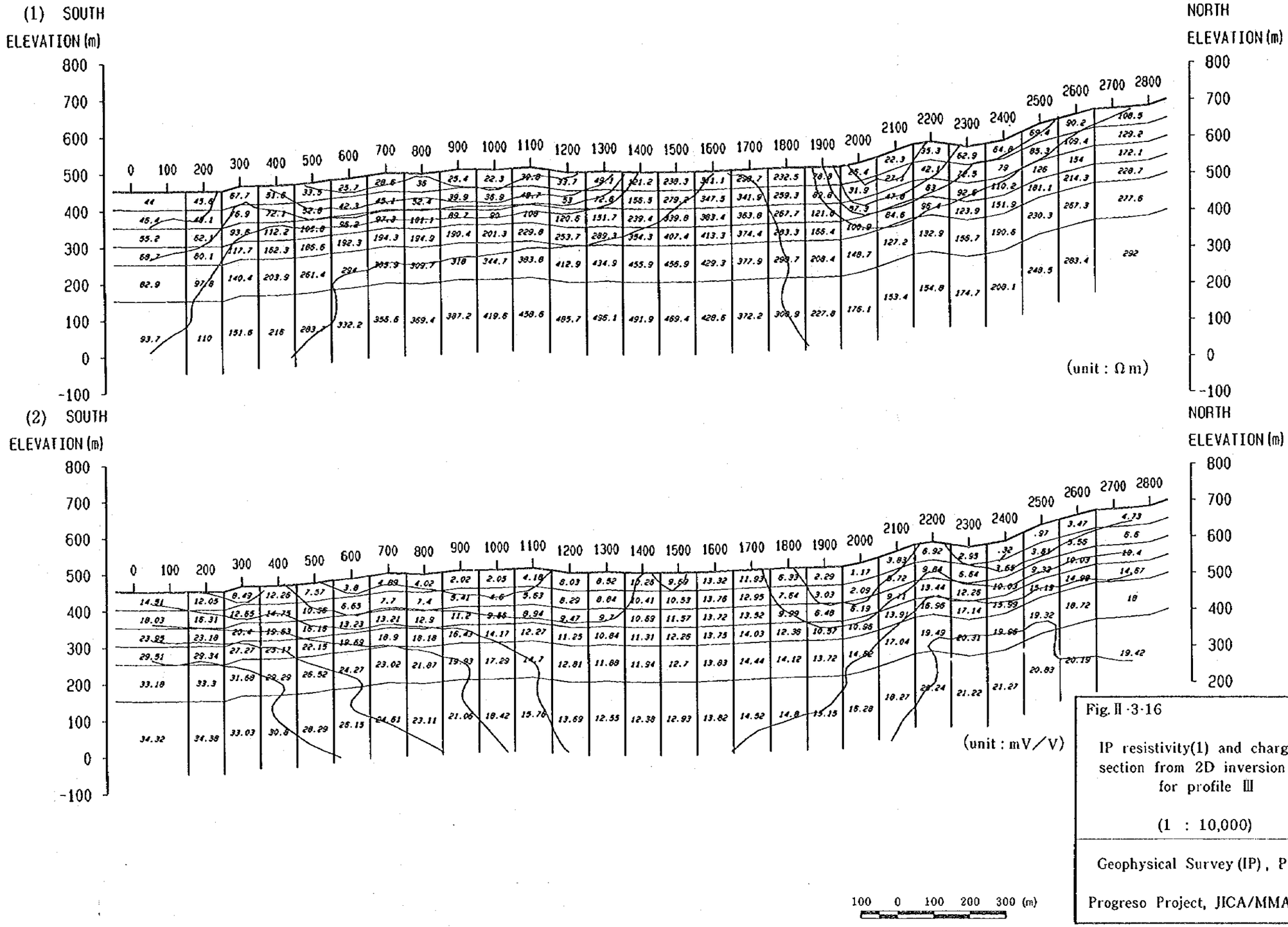

Fig. II-3-16

IP resistivity(1) and chargeability(2) section from 2D inversion result for profile III

(1 : 10,000)

Geophysical Survey (IP), Phase II

Progreso Project, JICA/MMAJ-ENAMI

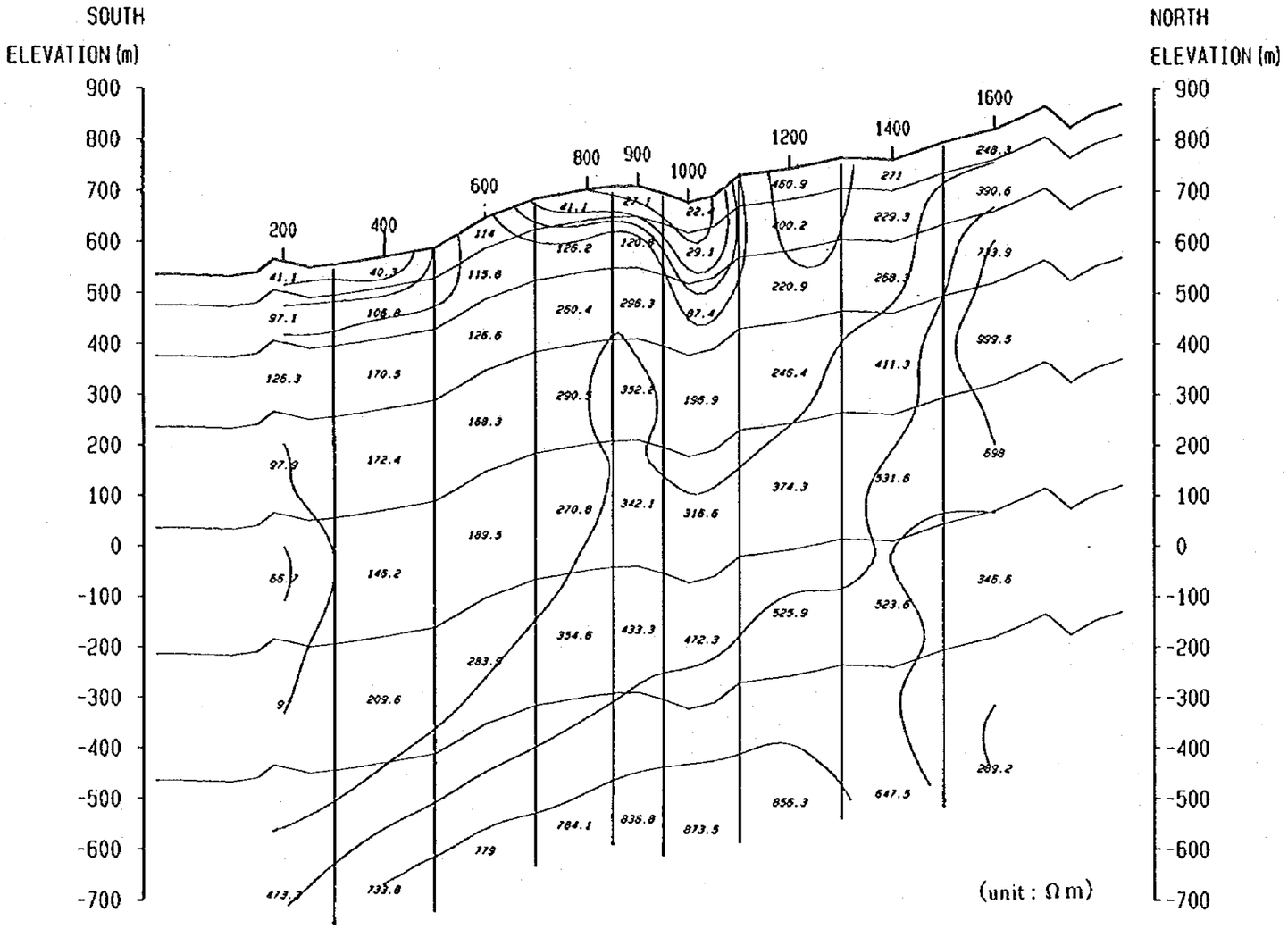

Fig. II·3·17

AMT resistivity section from 2D inversion result for profile III

(1 : 10,000)

Geophysical Survey (AMT), Phase II

Progreso Project, JICA/MMAJ·ENAMI

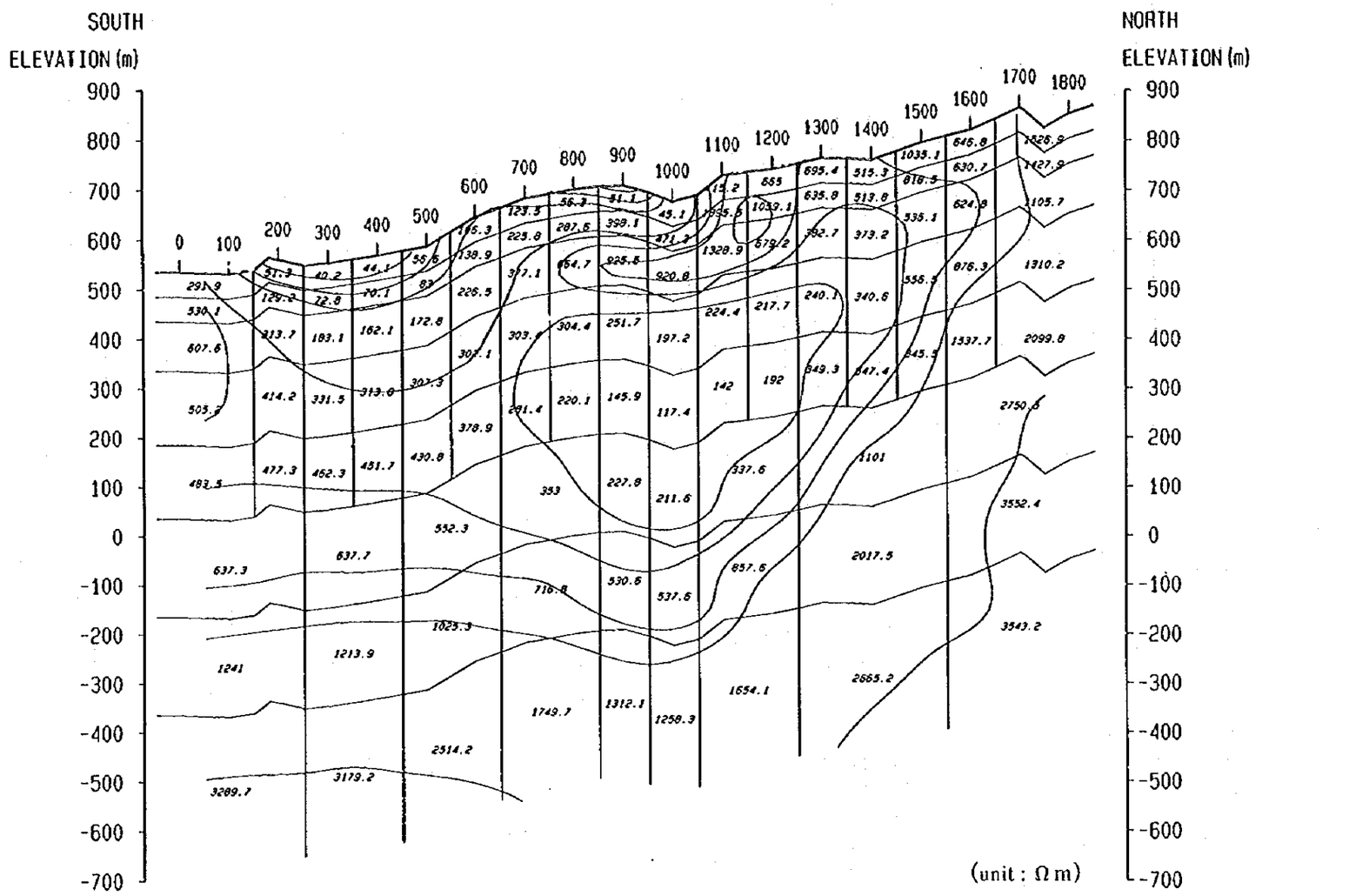

Fig. II-3-18(1)

Resistivity section from 2D joint inversion reslt for profile III

(1 : 10,000)

Geophysical Survey, Phase II

Progreso Project, JICA/MMAJ-ENAMI

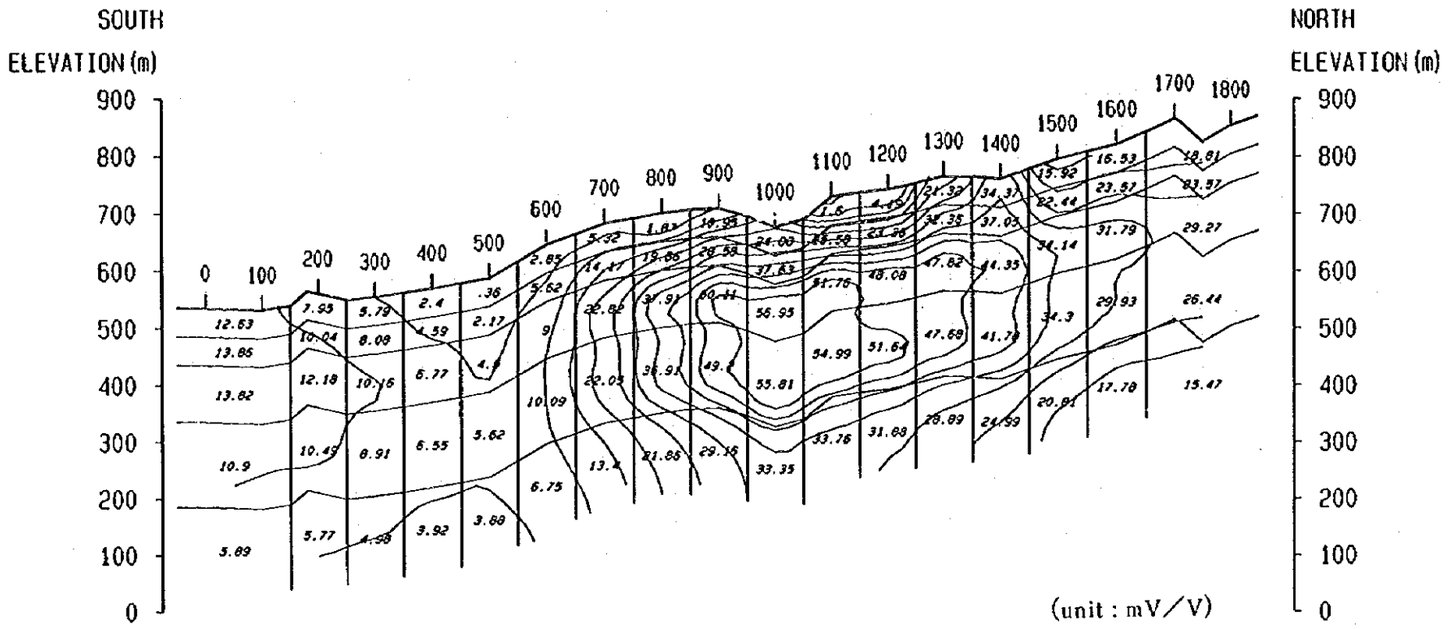

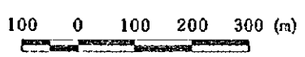

Fig. II -3·18(2)

Chargeability section from 2D joint inversion result for profile III

(1 : 10,000)

Geophysical Survey, Phase II

Progreso Project, JICA/MMAJ·ENAMI

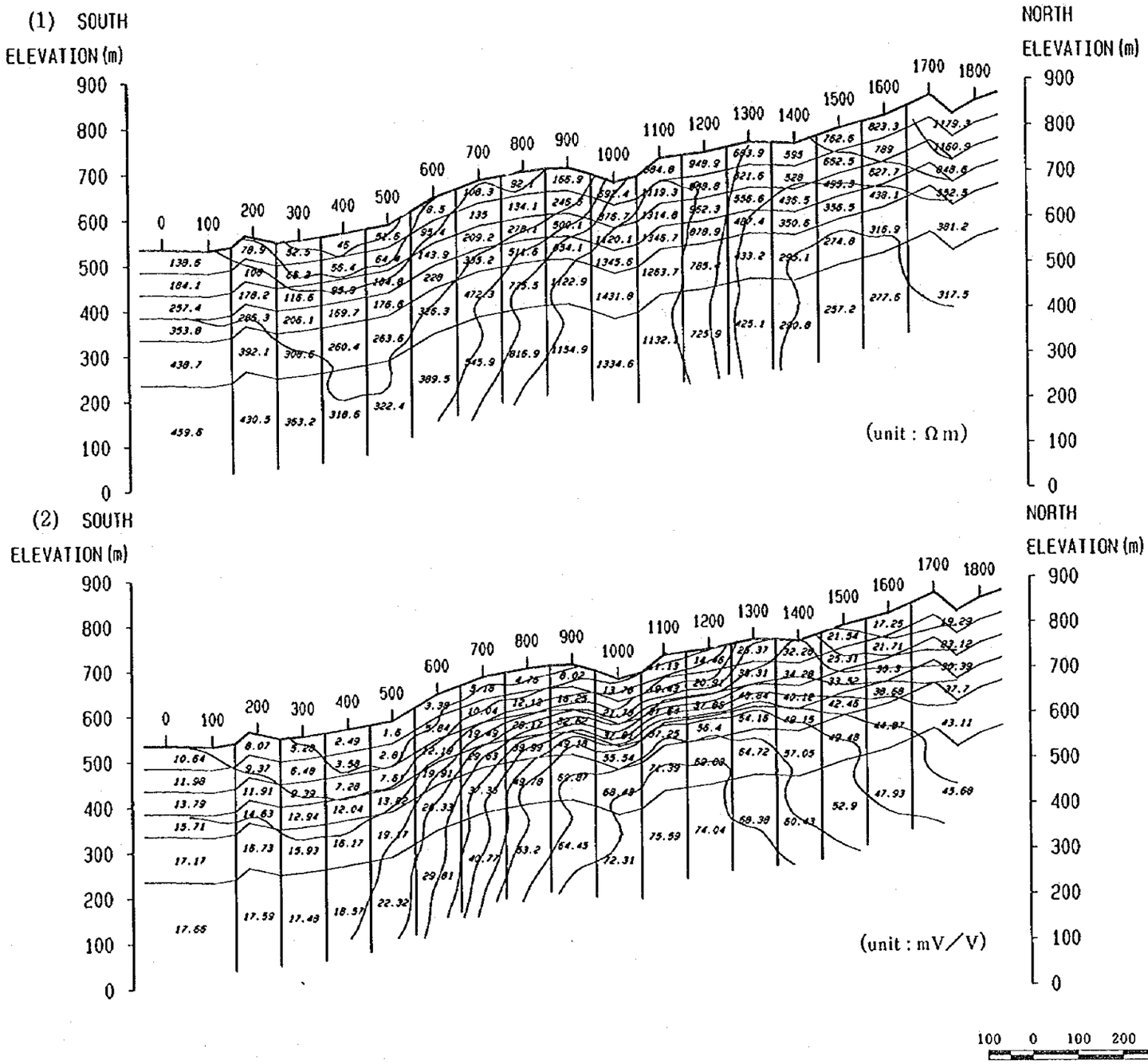

Fig. II-3-19

IP resistivity(1) and chargeability(2) section from 2D inversion result for profile Ⅳ

(1 : 10,000)

Geophysical Survey (IP), Phase II

Progreso Project, JICA/MMAJ-ENAMI

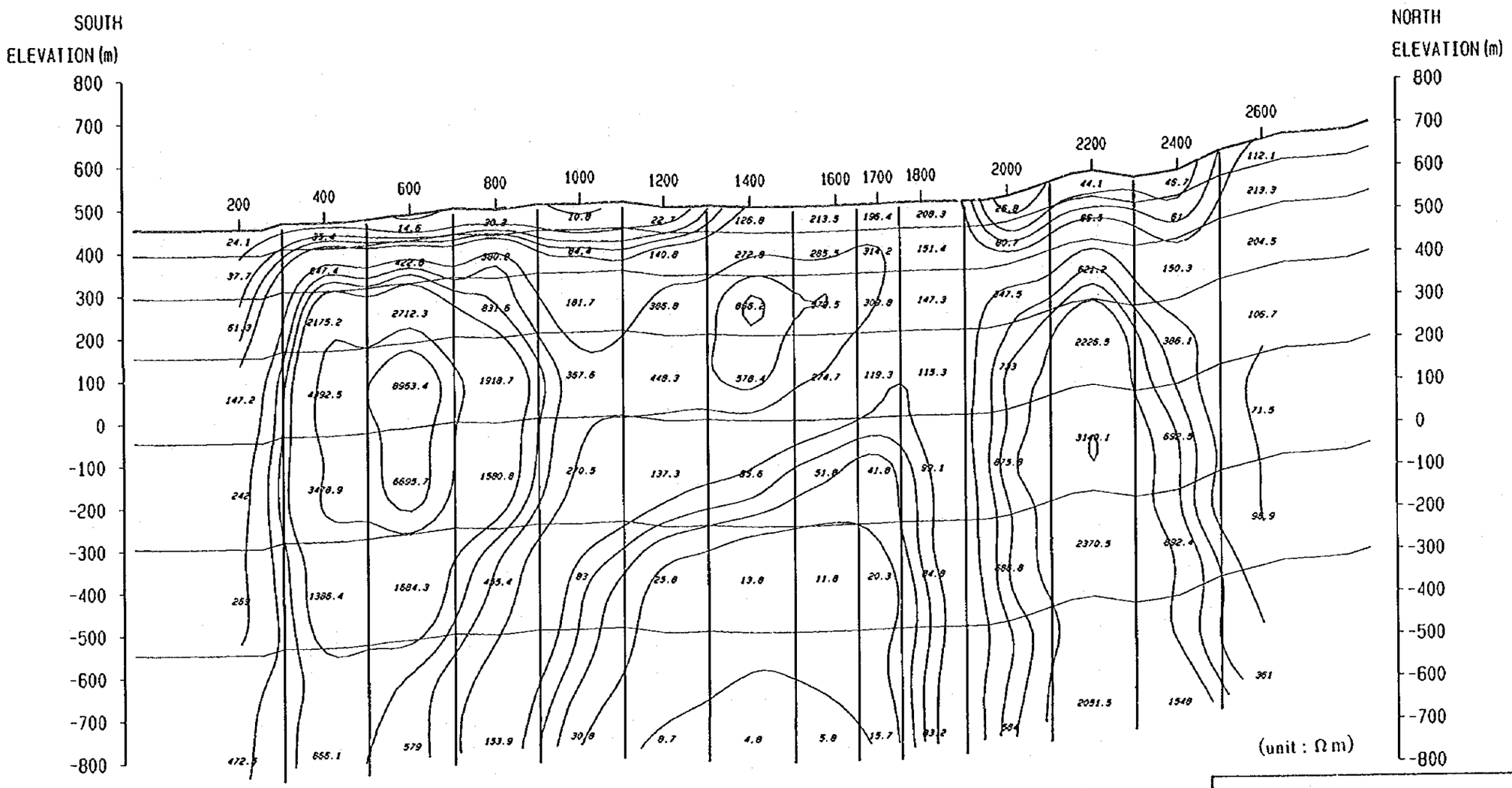

Fig. II-3-20

AMT resistivity section from 2D inversion result for profile IV

(1 : 10,000)

Geophysical Survey (AMT), Phase II

Progreso Project, JICA/MMAJ-ENAMI

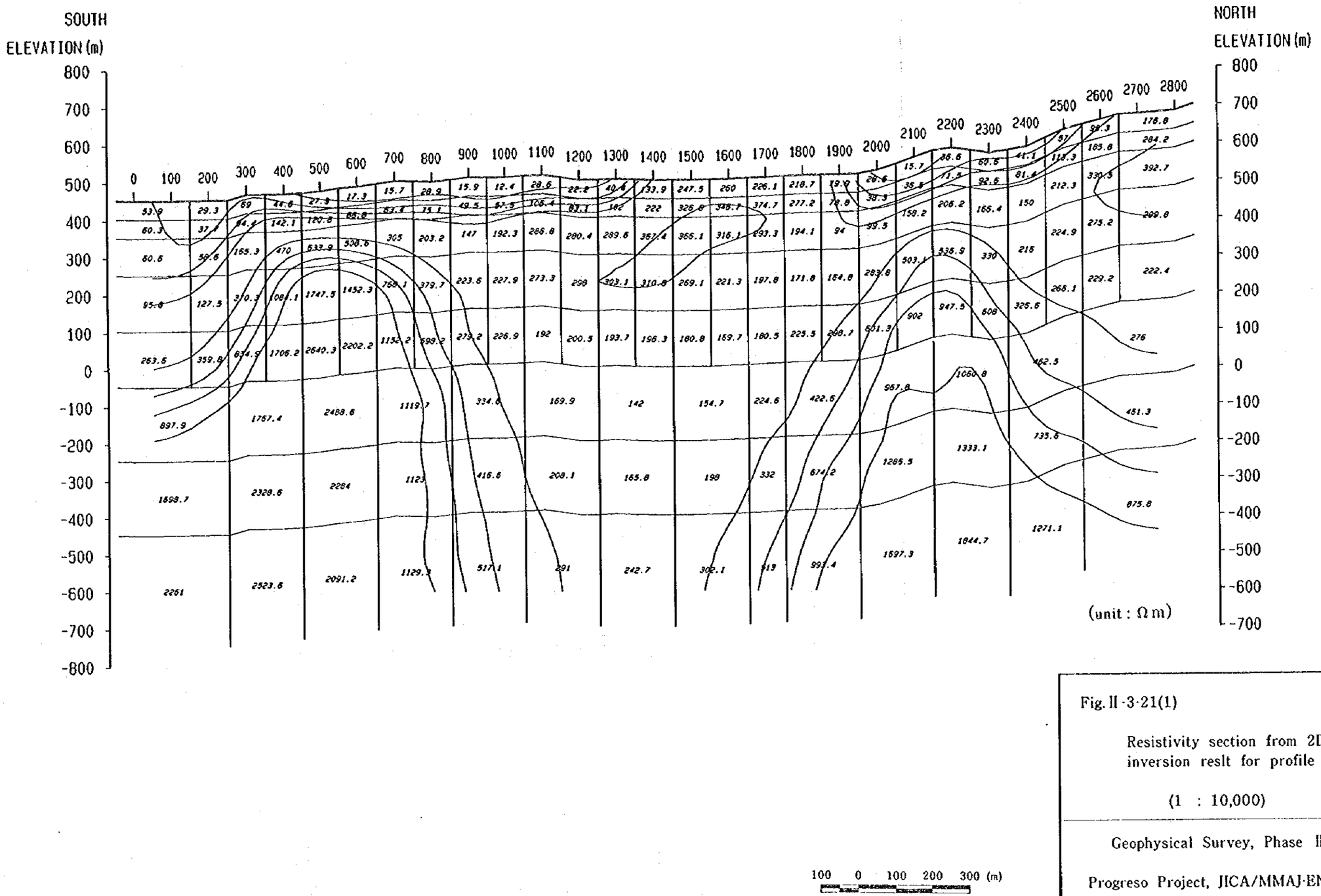

Fig. II-3-21(1)

Resistivity section from 2D joint inversion reslt for profile IV

(1 : 10,000)

Geophysical Survey, Phase II

Progreso Project, JICA/MMAJ-ENAMI

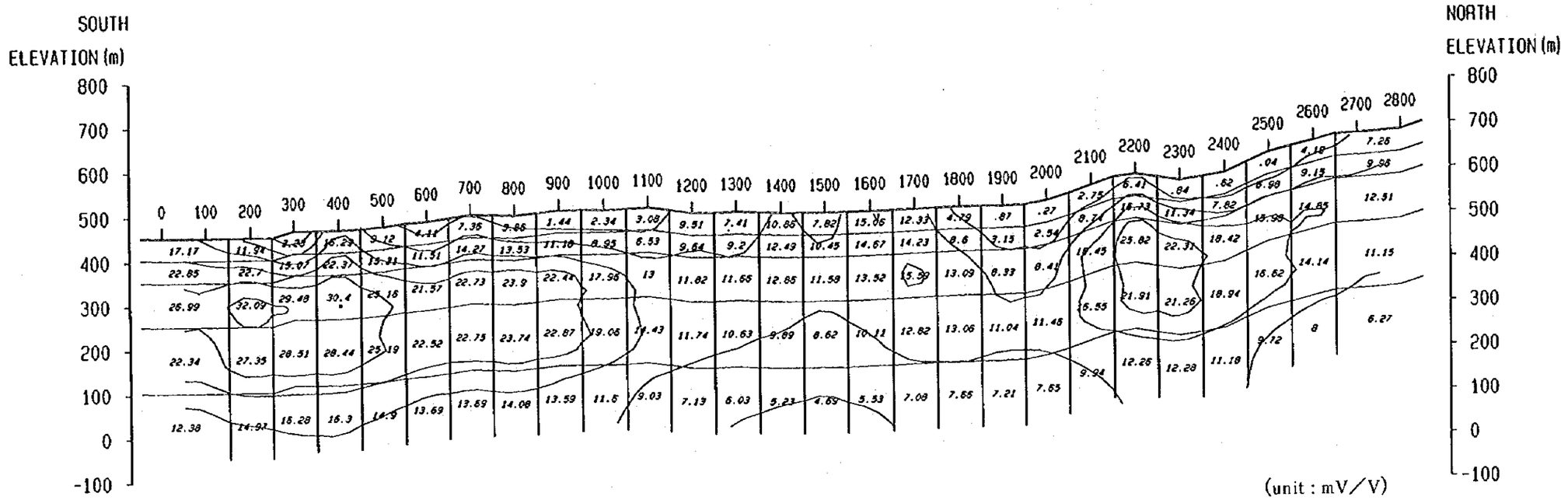

100 0 100 200 300 (m)

Fig. II-3-21(2)

Chargeability section from 2D joint inversion result for profile IV

(1 : 10,000)

Geophysical Survey, Phase II

Progreso Project, JICA/MMAJ-ENAMI

(1) WEST

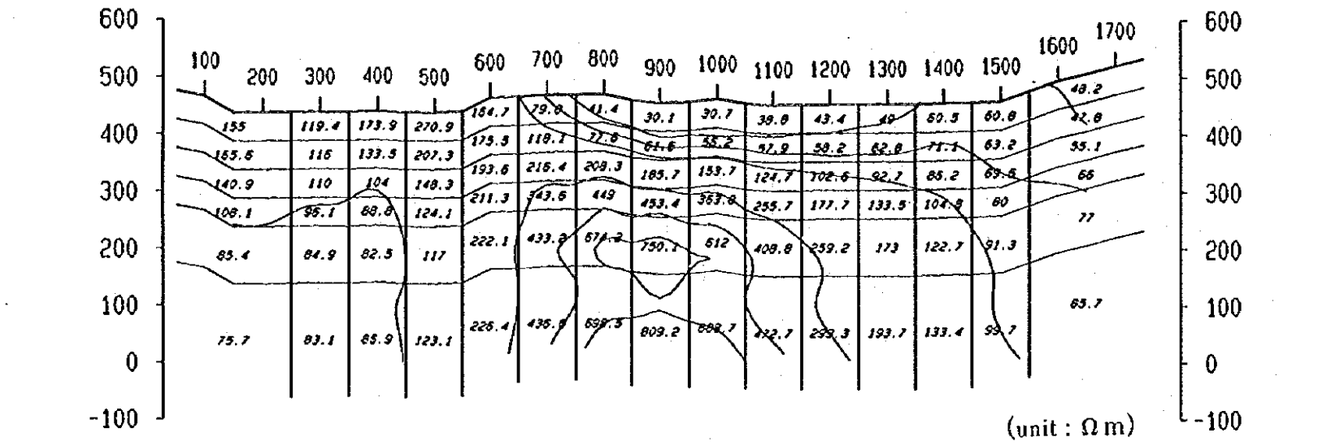

(2) WEST

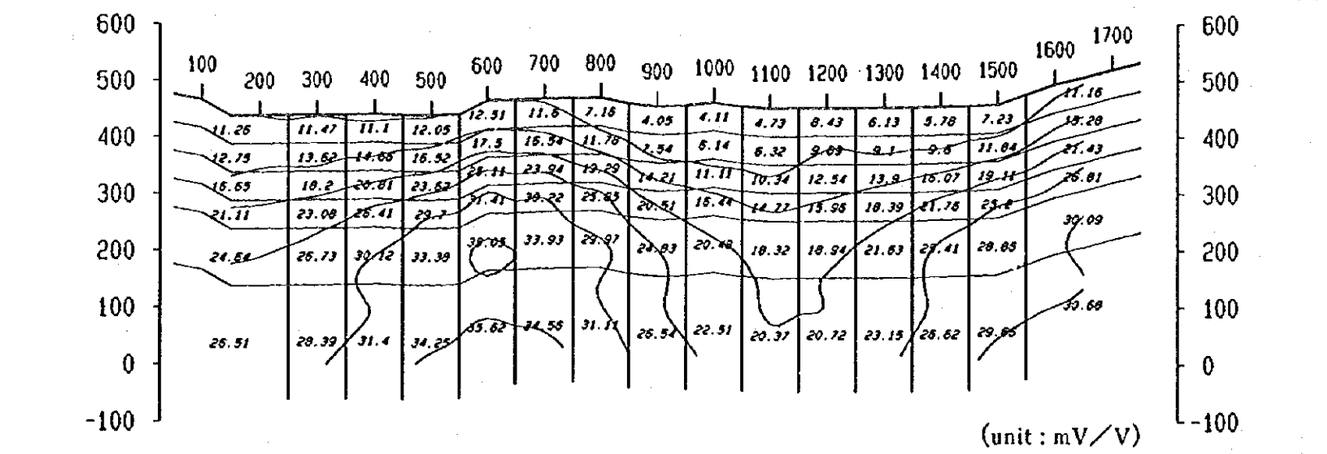

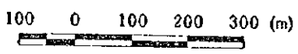

Fig. II-3-22

IP resistivity(1) and chargeability(2) section from 2D inversion result for profile V

(1 : 10,000)

Geophysical Survey (IP), Phase II

Progreso Project, JICA/MMAJ-ENAMI

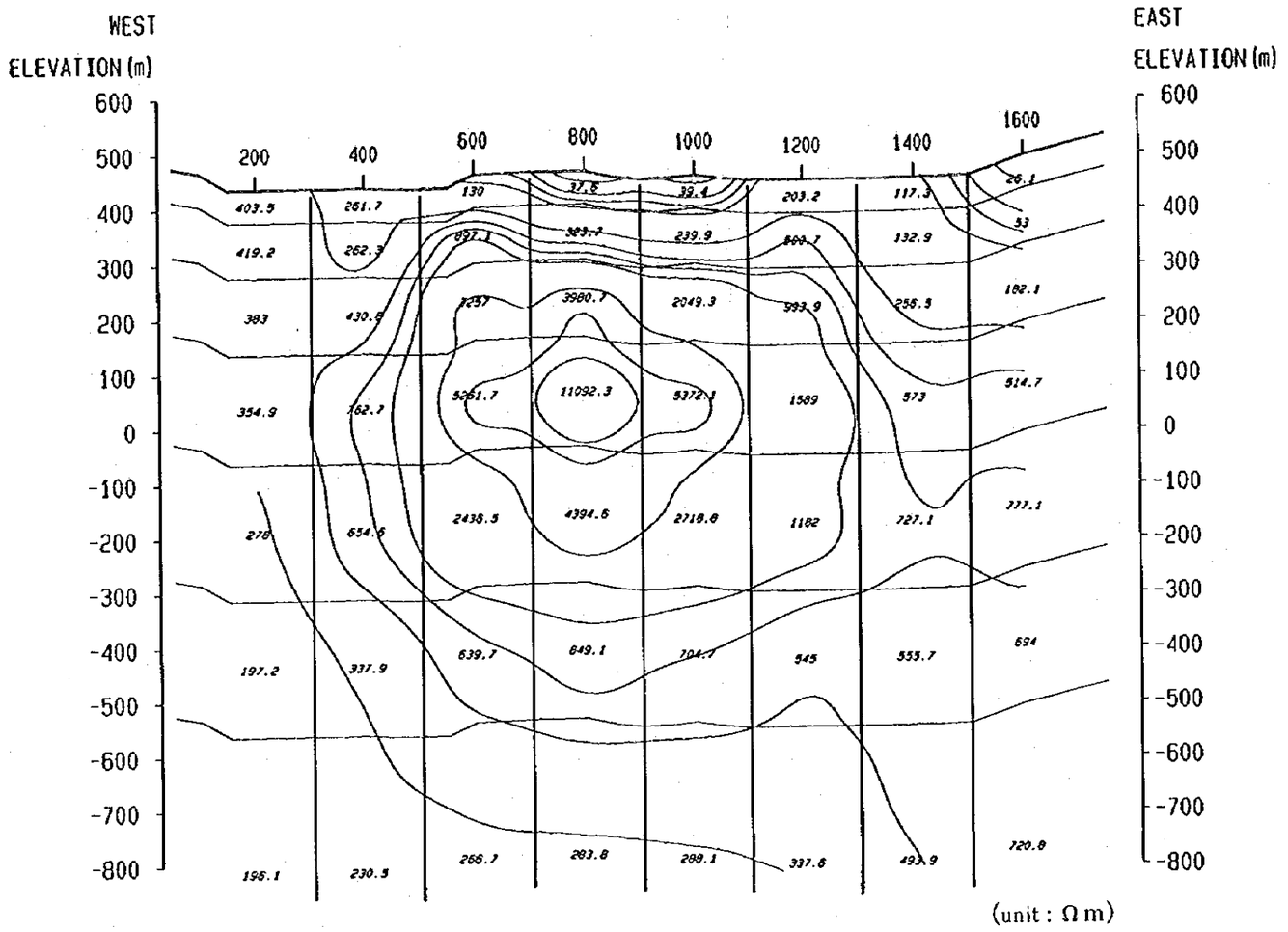

Fig. II-3-23

AMT resistivity section from 2D inversion result for profile V

(1 : 10,000)

Geophysical Survey (AMT), Phase II

Progreso Project, JICA/MMAJ-ENAMI

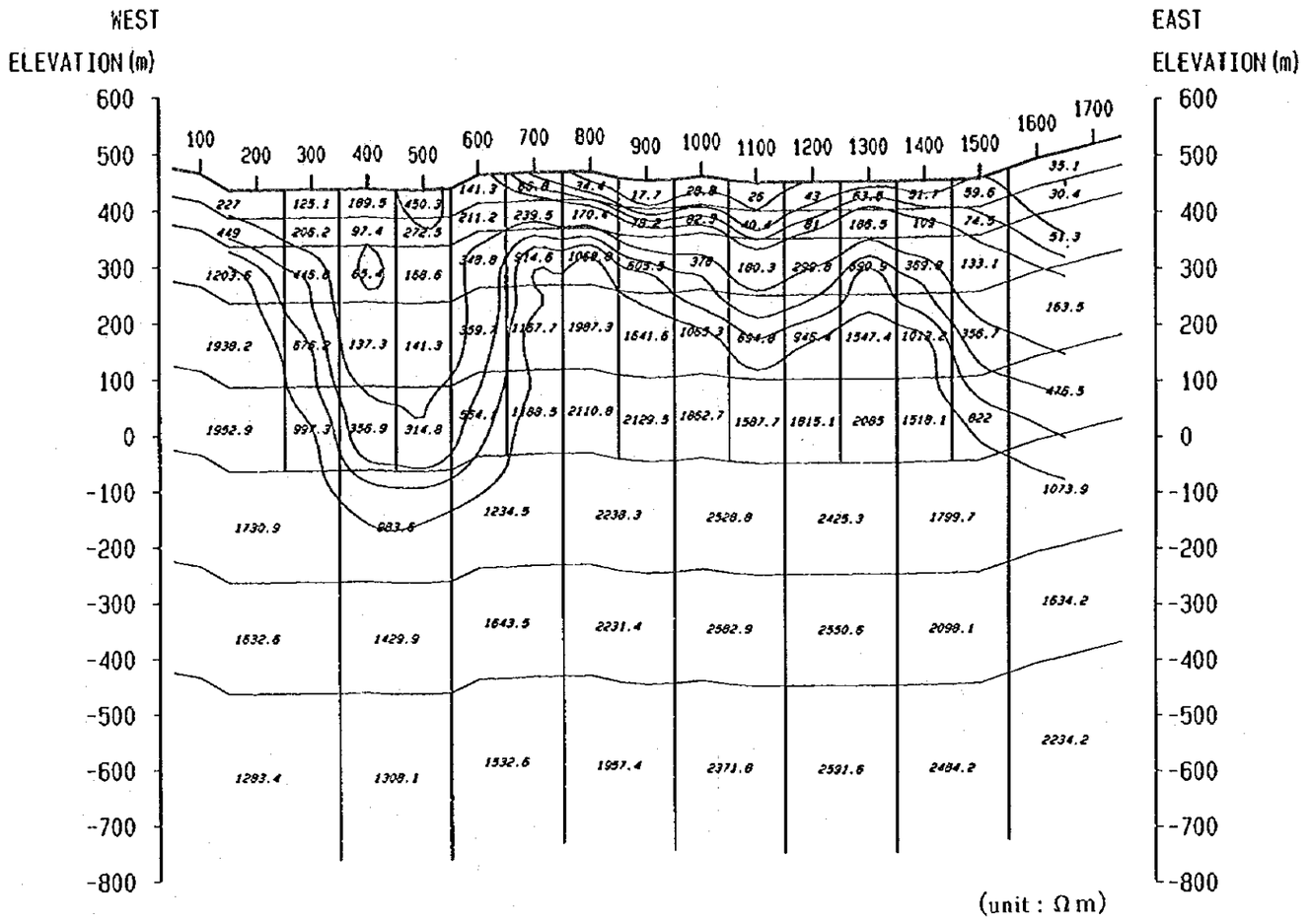

Fig. II-3-24(1)

Resistivity section from 2D joint inversion reslt for profile V

(1 : 10,000)

Geophysical Survey, Phase II

Progreso Project, JICA/MMAJ-ENAMI

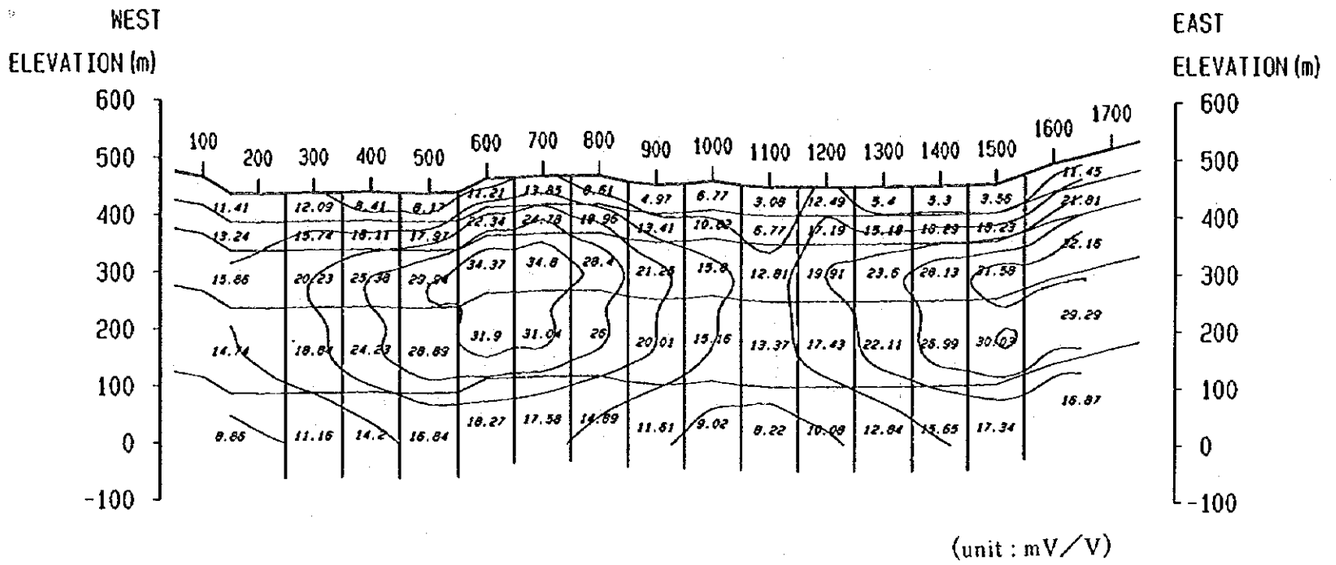

100 0 100 200 300 (m)

Fig. II -3-24(2)

Chargeability section from 2D joint inversion result for profile V

(1 : 10,000)

Geophysical Survey, Phase II

Progreso Project, JICA/MMAJ-ENAMI

800. Nevertheless, according to the results of joint inversion interpretation shown in Fig.II-3-24(1), resistivity values in the deep zone are around 1000Ωm to 2000Ωm, gradually dropping from alt. 300m to 400m between measurement points 600 and 1400, and from alt. 300m to 200m east of measurement point 1500, and falling to alt. 100m at measurement points 400 and 500. The resistivity structure in the shallow zone virtually corresponds to the results obtained by IP interpretation and a resistivity layer of less than 100 Ωm covers the surface east of measurement point 700.

According to the chargeability section obtained by the IP method shown in Fig.II-3-22(2), a chargeability zone of over 30mV/V is distributed from measurement point 400 to below measurement point 800 and below measurement point 1600. According to the results of joint inversion interpretation shown in Fig.II-3-24(2), a zone extending downwards from measurement point 500 to measurement point 700 and from measurement point 1500 to measurement point 1700 is distributed in limited form.

3-4 Considerations

The geology around the survey area consists of lower Cretaceous volcanic rock and sedimentary rock, intrusive rock thought to have been active from the Middle Cretaceous to the Early Tertiary, and Pleistocene and Holocene unconsolidated sediment. The lower Cretaceous volcanic rock and sedimentary rock can be classified from below as Punta del Cobre formation, Abundancia formation, Nantoco formation and Bandurrias formation. Punta del Cobre formation and Abundancia formation are distributed in the survey area.

The Punta del Cobre formation can be classified into lower and upper strata. The lower formation is mainly composed of andesitic lava and the lower limit has not been confirmed. The upper layer is 60 - 120m thick and consists of andesitic lava, andesitic tuff breccia, lapilli tuff and tuff volcanic rock, with intercalated beds of sedimentary rock such as slate, sandstone, calcareous sandstone and limestone. Andesite and albitized meta-andesite are exposed in the upper layer, but for the most part they are covered by the Quartenary formation.

The Abundancia formation covers the Punta del Cobre formation and from below consists of a stratified limestone-prominent formation, a weak formation-massive limestone formation intercalated with trachytic tuff, and skarn accompanied by mineralization.

The intrusive rocks consist of Andes batholith granite and veins of intrusive acid to basic rock.

Metal deposits in the environs of the survey area can be classified into three types: (a) Manto-type ore deposits whose parent rock is the Punta del Cobre formation, breccia-type ore deposits and vein-type deposits (chalcopyrite-pyrite magnetite - hematite ore), (b) Manto-type ore deposits whose parent rock is the Abundancia formation garnet skarn and hornfels (gold-bearing oxidized copper-chalcopyrite ore), and (c) gold-bearing iron ore vein-type deposits whose parent rock is Andes batholith.

The results of the survey did not reveal the areas of anomaly showing low resistivity-high chargeability

that had initially been forecast. In the laboratory measrements on boring cores it was found that the samples from this area showing a high chargeability tended on the whole to display a high resistivity. Values measured in samples taken from DDH-1A and DDH-6A, where the Punta del Cobre formation, a horizontal ore deposit, has been verified, displayed high resistivity values of over 800 Ω m(average resistivity 10,635 Ω m). While the lack of boring data actually striking deposits in this area makes it difficult to be certain, it is thought probable that actual Manto-type deposits do have a low resistivity-high chargeability, and it was not possible from the results of this survey to extract any such marked anomaly. However, the high resistivity-high chargeability anomaly either arises from a garnet skarn of the Abundancia formation accompanying mineralization, or the resistivity of the andesite which is the country rock of the Punta del Cobre formation is extremely high and the influence of this was observed in the surface measurements as high resistivity-high chargeability. If this is the case, we cannot expect to find large scale deposits of minerals, but the question can be considered a survey index.

In DDH-1A (Fig.II-3-25(a)), the alluvials core sample shows a resistivity value of less than 100 Ω m, and a resistivity value of over 800 Ω m is shown in the Punta del Cobre formation below 188.6m. Moreover, in DDH-6A (Fig.II-3-25(c)), a resistivity value of over 1000 Ω m is shown in both the Abundancia formation up to a depth of 474m and the Punta del Cobre formation over a depth of 474m. In DDH-1 (Fig.II-3-25(b)), granodiorite is distributed below a depth of 103.6m. The resistivity values are slightly low at 200-300 m in places assumed to have been affected by weathering between 103.6m and 137.1m deep, but a value of over 1500 Ω m is shown below a depth of 137.1m. It is therefore considered difficult to separate the Punta del Cobre formation and the Abundancia formation above it by resistivity values. However, as the resistivity values of the alluvials are low and the difference is clear, it is possible to clarify the geologic structure of the survey area by tracing the structure of the high resistivity values. Moreover, looking at the correspondence between the chargeability of core samples and copper analysis values, the high chargeability core samples have the high copper analysis values from depths of 72m and 140m in DDH-6A.

Taking an overall view of the resistivity structure of this area, the height of the top of the resistivity layer of over 300 Ω m is shown on the plane figure from the results of two-dimensional joint inversion interpretation. Moreover, measurement points where chargeability is over 30mV/V and over 50mV/V are shown in Fig.II-3-26. As for the tendencies of the resistivity structure of the entire area, on the east side the high resistivity zone tends to be shallow and on the west side it tends to be deep. In the north, taking profile II measurement point 1400 as the boundary, the high resistivity zone becomes rapidly deeper on the north side and the existence of a fault is assumed. In the east, the high resistivity zone juts out from profile III measurement point 800 towards profile IV measurement point 2200, and the existence of intrusive rocks is assumed from this structure. In the south, the high resistivity zone becomes shallow on the south side linking profile V measurement point 500 and profile IV measurement point 800, and then becomes deep

again on the south side linking profile V measurement point 1100 and profile IV measurement point 400. From the range of the present measurements it is impossible to ascertain whether this tendency extends over the entire south side of the survey area or is a local drop. The high resistivity zone on the west side from profile V measurement point 200 is shallow. This is an area in which geologically also the Abundacia formation is distributed on the surface, so that both results agree.

As described above, anomalies indicating marked mineral prospects with a low resistivity-high chargeability were not found in this area. However, assuming that the high resistivity-high chargeability anomaly indicates a skarn mineral deposit, or indicates a structure in which the Punta del Cobre formation is distributed near the surface and is accompanied by the mineralization effect, the chargeability is over 50mV/V are laid over the a shallow region of a high resistivity zone is thought to be an effective indicator of mineral prospects in the survey area. Tow regions can be extracted, the region centering on profile II measurement point 1300 in the central eastern part of the area and the region centering on profile III measurement point 1000. In addition, a region with high chargeability centering on profile II measurement point 2000 in the northeast of the area was confirmed. While no rise in the zone of high resistivity is assumed, a region of high chargeability was observed; this is a region close to a high anomaly zone measured in the airborne magnetic survey, and it is hoped that these areas will be subjected to further surveys.

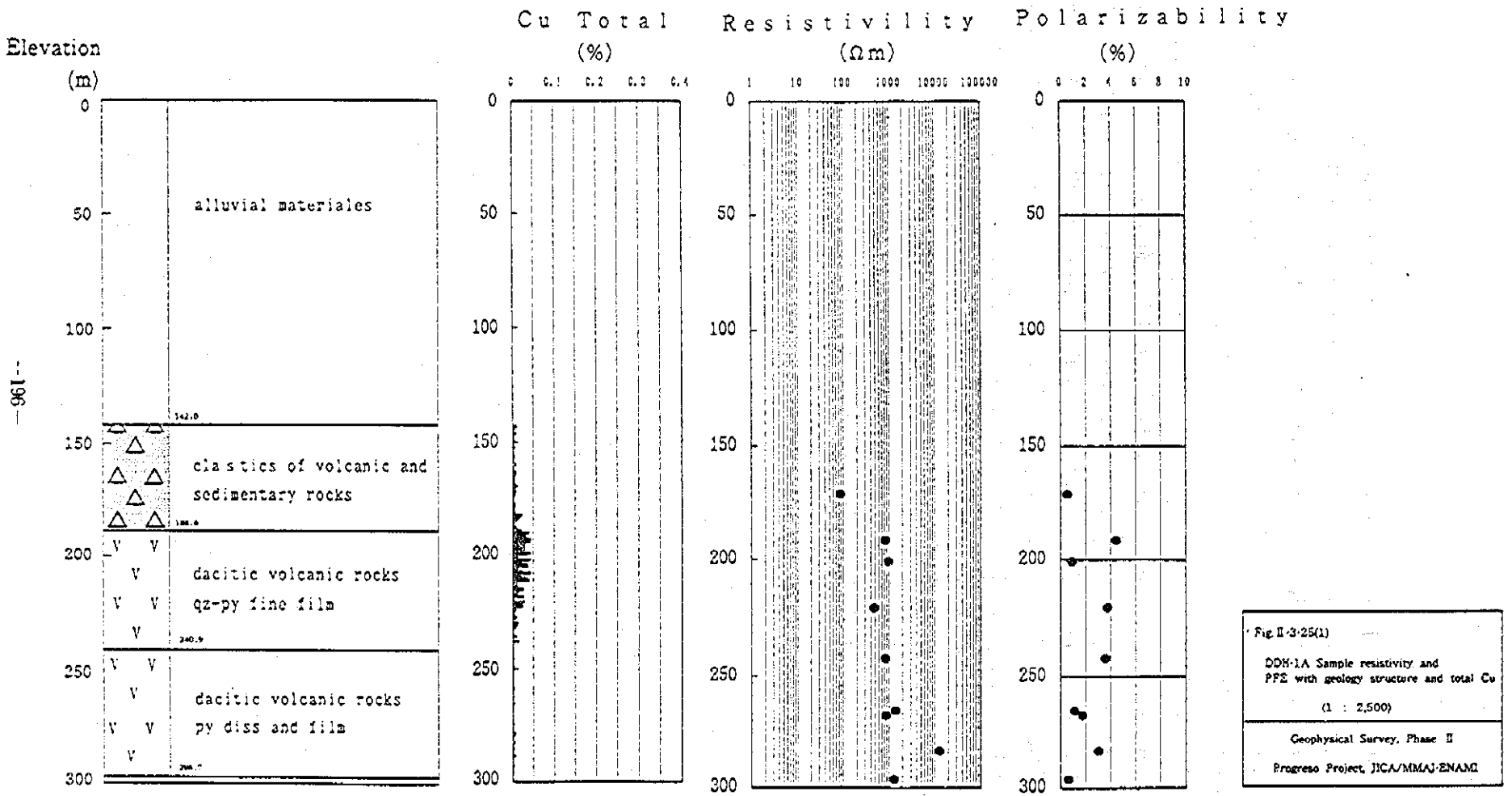

Fig. II-3-25(1)

DDH-1A Sample resistivity and PFE with geology structure and total Cu

(1 : 2,500)

Geophysical Survey, Phase II

Progreso Project, JICA/MMAJ-ENAMI

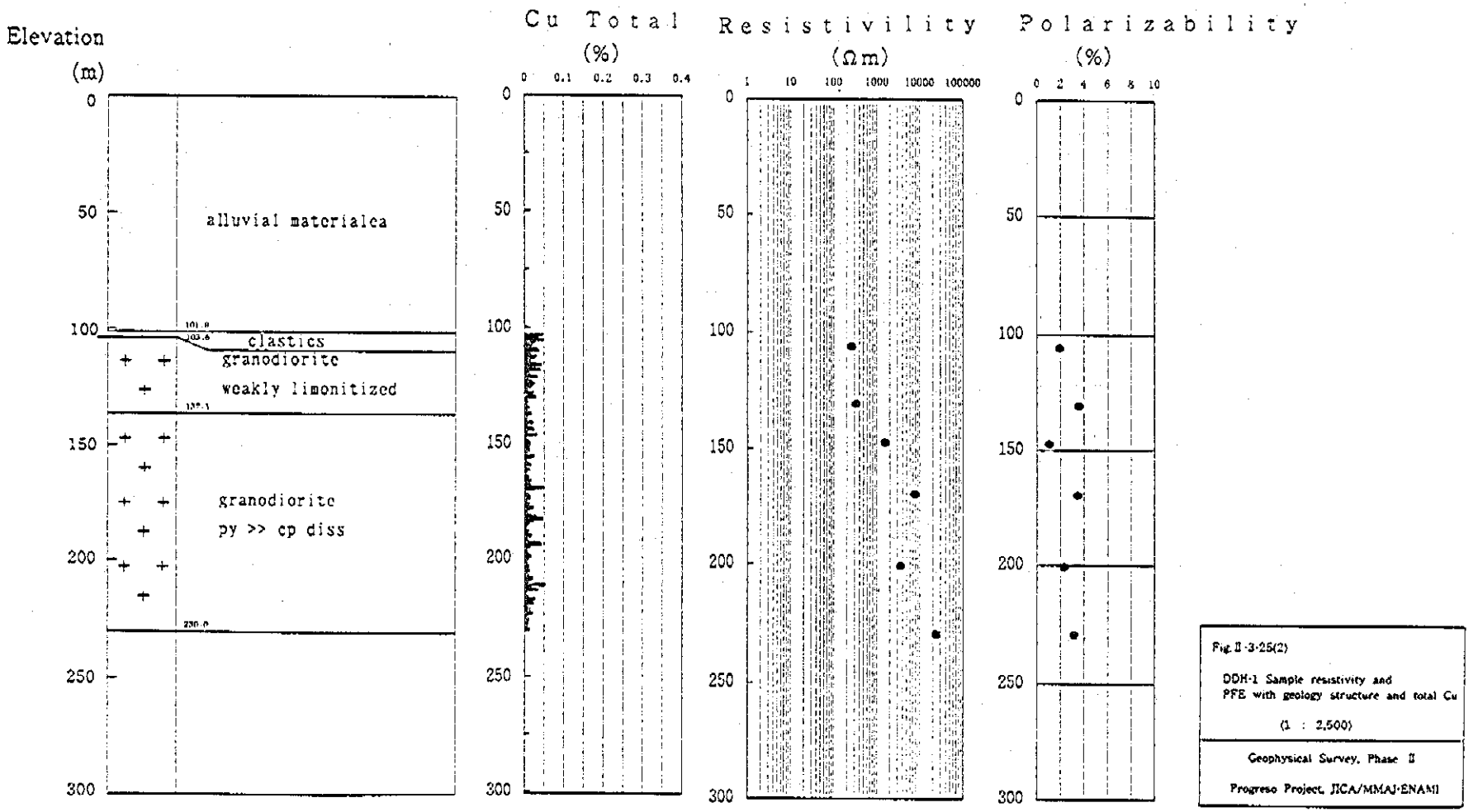

Fig.Ⅱ-3-25(2)

DDH-1 Sample resistivity and PFE with geology structure and total Cu

(1 : 2,500)

Geophysical Survey, Phase Ⅱ

Progreso Project, JICA/MMAJ-ENAMI

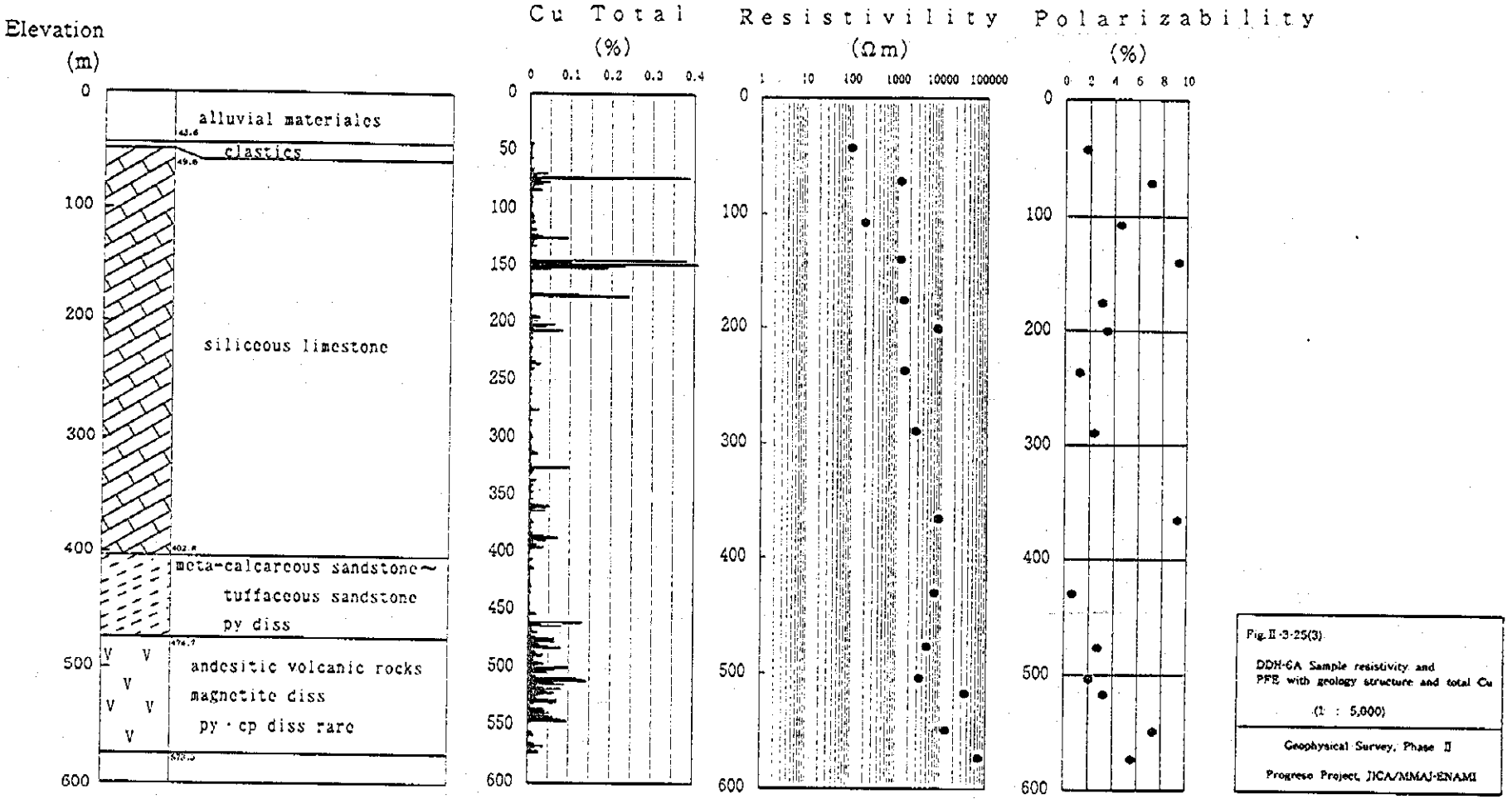

Fig.II-3-25(3)

DDH-6A Sample resistivity and PFE with geology structure and total Cu

(1 : 5,000)

Geophysical Survey, Phase II

Progreso Project, JICA/MMAJ-ENAMI

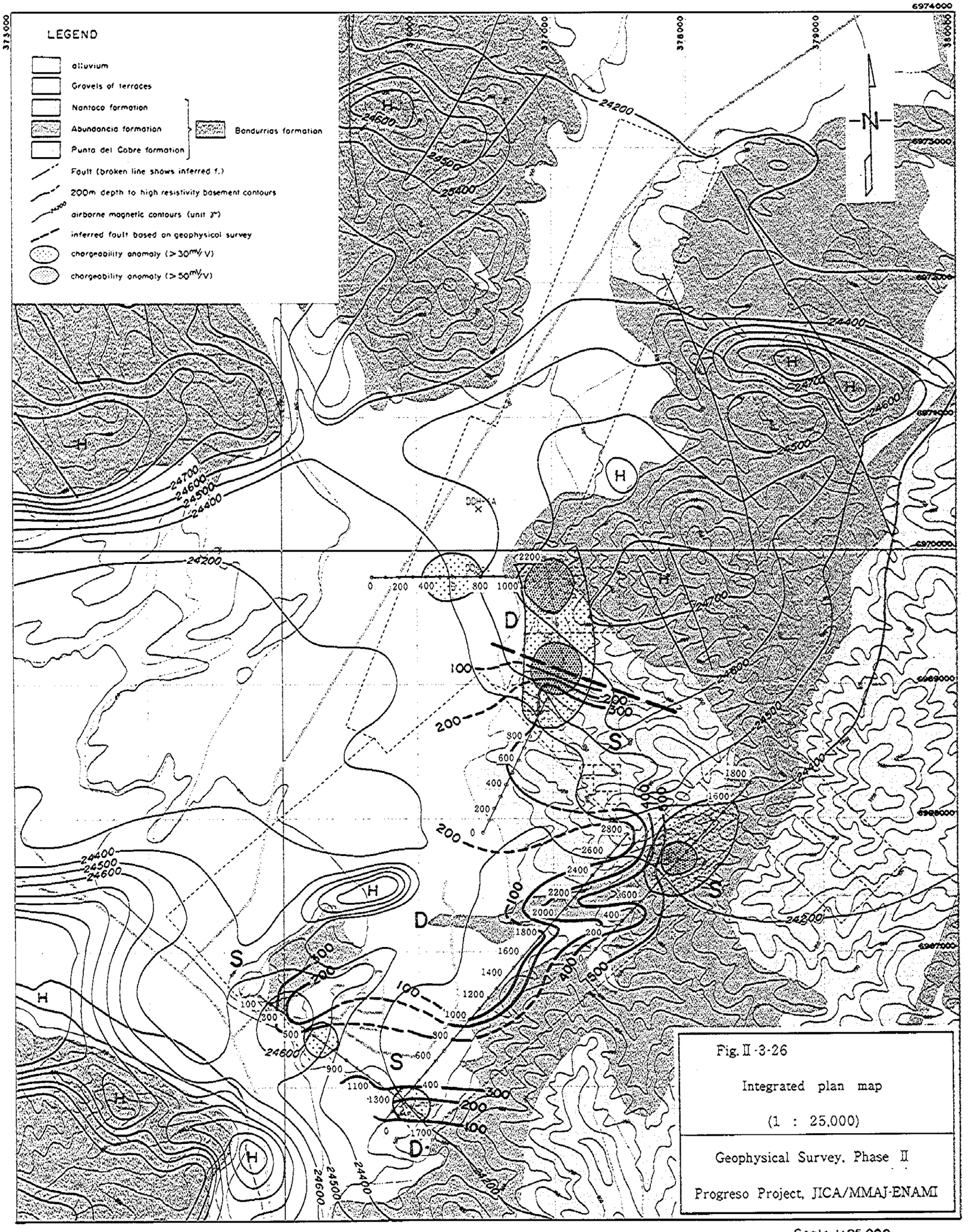

Fig. II-3-26

Integrated plan map

(1 : 25,000)

Geophysical Survey, Phase II

Progreso Project, JICA/MMAJ-ENAMI

Scale 1:25,000

0 500 1,000m

PART III CONCLUSION AND RECOMMENDATION

PART III CONCLUSIONS AND RECOMMENDATIONS

CHAPTER 1 CONCLUSIONS

The conclusions reached from the second phase of the Cooperative Mineral Exploration in the Veraguas-Progreso areas of the Republic of Chile, are asfollows.

1-1 Drilling Survey in the Veraguas Area

1. Sierra Overa District

The district is made up of andesite volcanics with intrusive diorite/andesite porphyry, both rocks having undergone strong hydrothermal alteration. The district has fractures running in N-S and NW-SE directions, and it may be considered that these fractures acted as channels for the porphyry intrusion. In articular, the porphyry stock striking NW-SE and ranging in width 100-200m is exposed in the north-western hillside of the Sierra Overa. In the district, the surface stratum and along the above-mentioned fractures forms a leached zone 10 to 200m thick made up of a strongly silicified zone, a quartz-sericitized zone and a siliceous argillized zone with strong concentrations of jarosite and reddish hematite.

Below the leached zone, the alteration is divided into a siliceous argillized zone and a chloritized zone. The chloritized zone has marked pyrite dissemination and is further divided, from the top down, into four zones; siliceous argillized-chloritized zone, chloritized zone ,silicified-chloritized zone and silicified-chloritized-potash feldspar zone. From this mineral association, it may be considered that the first three zones correspond to the phillic zone, and the fourth zone to the potassic zone of the alteration classfication of porphyry copper deposits by Lowell and Guilbert (1970).

In the northwestern hillside of the Sierra Overa, MJCV-13 revealed a mineralized zone containing copper oxides, native copper, chalcopyrite and small amounts of covelline, chalcocite and bornite in the diorite porphyry. The mineralization and alteration show the following correspondence.

Depth	Cu mineral	Cu ave.	max.	Auppm	Alteration
0- 11m	atacamite/brochanthite	0.55%	1.24%	0.20	siliceous argillized-chloritized
11- 70m	atacamite/brochanthite	0.24	1.12	0.14	chloritized
70- 78m	atacamite/brochanthite	0.34	0.40	0.21	chloritized
78-149m	Cu'-atacamite-azurite	0.23	0.86	0.13	chloritized
149-180m	Cu'-atacamite-azurite	0.18	0.52	0.13	silicified-chloiritized-potash feldspar
180-198m	atacamite-azurite	0.14	0.27	0.09	silicified-chloiritized-potash feldspar
198-250m	chalcopyrite	0.11	0.26	<0.04	silicified-chloiritized-potash feldspar
250-300m	chalcopyrite	0.10	0.55	<0.04	silicified-chloiritized-potash feldspar

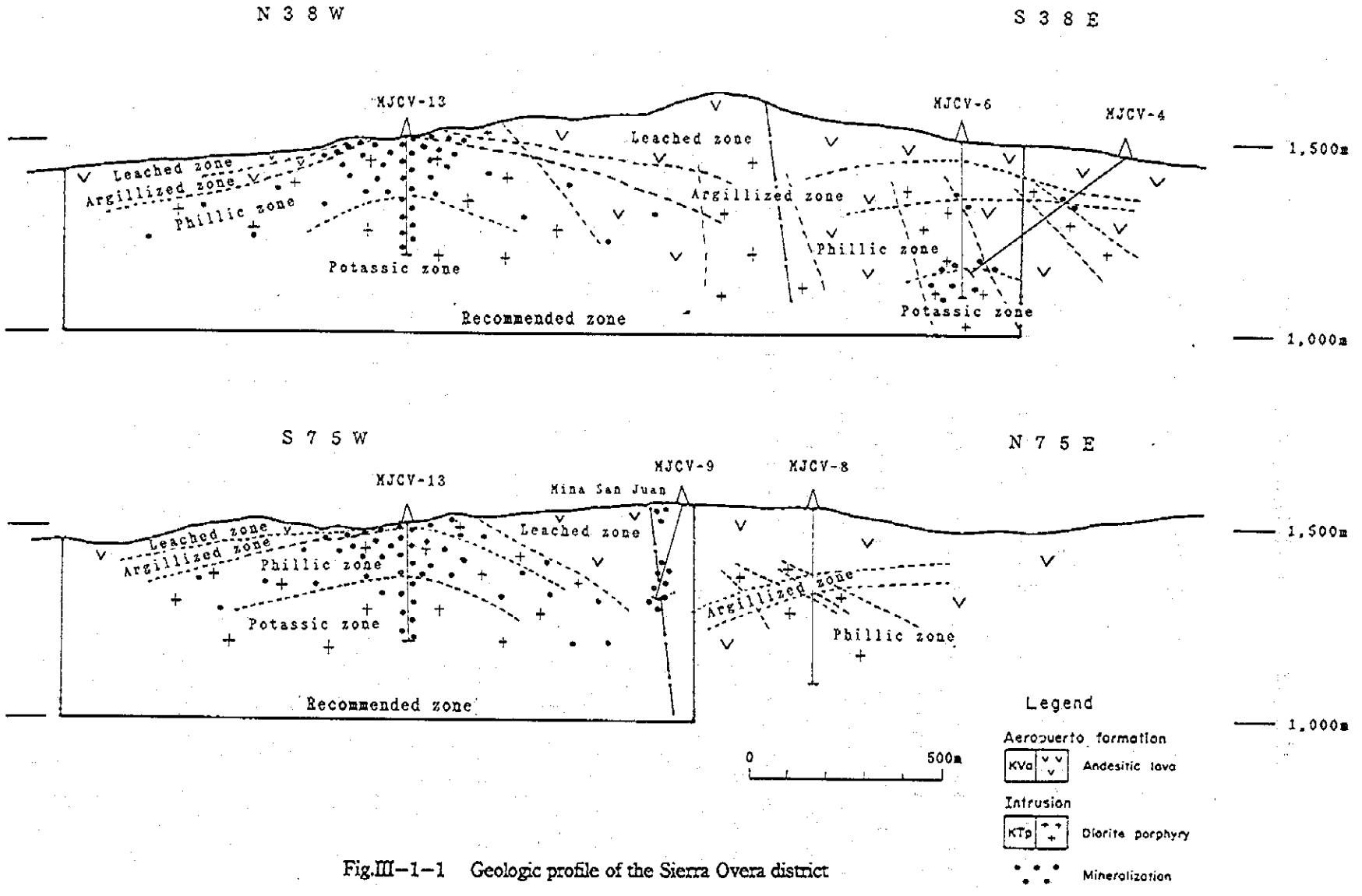

Fig.III—1—1 Geologic profile of the Sierra Overa district

In the phillic zone between 0-149m, the T.Cu grade is >0.2% and the Au grade >0.1ppm, but in potassic zone below 149m , the mineralization of copper and gold tends to weaken.

Native copper occurs in disseminate and film form between 78-180m, and observation under the microscope reveals small amounts of chalcopyrite and bornite with native copper. In addition to the above-mentioned copper minerals, hematite and magnetite also occur universally. In places where native copper occurs the hematite has not completely replaced the magnetite,

and both associate together. In places where copper oxides are abundant, the replacement of magnetite by hematite is more advanced.

In addition, from MJCV-6 chalcopyrite dissemination was found accompaning the potassic zone deep under the eastern side of the Sierra Overa, and from MJCV-9 copper oxide dissemination was found accompanying the leached zone of the north of the Sierra Overa, where the San Juan mine is located.

Thus it may be expected that porphyry copper deposits would be embedded under the leached zone that forms the Sierra Overa, and there is a need to continue further prospecting.

2. Cerro Veraguas District

This area is made up of andesite volcanics with intrusive diorite-andesite porphyry, both of which, like the Sierra Overa area, have undergone strong hydrothermal alteration. The district has fractures running in NE-SW and NW-SE directions, and it may be considered that these fractures acted as channels for the porphyry intrusion. In the eastern part of the Cerro Veraguas, MJCV-11 found a mineralization approximately 2m wide with a T.Cu grade of 0.76%, made up of covelline and chalcocite accompaning a pophyry assumed to have intruded regulated by the NW-SE fracture. Thus it may be expected that in the eastern part of the Cerro Veraguas district the porphyry copper deposits would be embedded controlled by the NW-SE structure, albeit on a small scale.

However, in the area from the center to the western part of the Cerro Veraguas, although drilling in the first year and this year revealed localized copper mineralization in the range of 0.2% to 0.7%, the poor continuity suggests that widespread mineralization is not to be expected.

Also the plain to the south of the Cerro Veraguas is covered to a depth of approximately 200m with andesite volcanics and volcanic sandstone of the Paleogene Chile-Alemania formation that has not undergone alteration, so the existence of mineralization is not expected.

3. Pampa District: the Plain east of the Cerro Veraguas

Quartz diorite stock, which NW-SE liniation is developed, is distributed over a range 2 x 2km. The rock yields copper oxide and chalcopyrite in film and disseminate form, accompanied by hematite, chlorite, epidote, quartz and calcite. This mineralized zone is thought to be stockwork deposits, controlled by the NW-SE structure. The one or two kilometres between the district and the Cerro Veraguas are covered

by alluviums and colluviums and the borders between the quartz diorite stock and the andesite volcanics of the Aeropuerto formation is not distinct. And the genetic relationship between the mineralization and the porphyry copper type mineralization is not apparent. These points should be further surveyed.

4. K-Ar Dating

K-Ar dating was carried out on the dioritic porphyry of the Sierra Overa area and on the quartz diorite of the Pampa area which had undergone mineralized alteration. The results are as follow;

The results are as follows;

Diorite porphyry(Sierra Overa east district)	: 104.0±+2.0Ma
Diorite porphyry(Sierra Overa northwest district)	: 115.0±+4.0Ma
Quartz diorite(Pampa District)	: 93.8±+2.1Ma

1. K-Ar ages indicate them to be Cretaceous in age. The diorite porphyry of the Sierra Overa district has undergone either phillic and potassic alteration, which displays the alteration pattern of porphyry copper deposits, while the quartz diorite of the Pampa district is characterized by chlorite, epidote and calcite, which displays the typical alteration of vein and stockwork type deposits found widely in the coastal cordillera ; but there is little difference in the period in which both underwent mineralizing alteration.

2. Since the K-Ar ages of the Grupo Plutonico Cerro del Pingo,which have a wide distribution over the coastal cordillera, indicate 109-121Ma (Naronjo et. al., 1984), the period of the mineralizing alteration corresponds roughly to that of the activity of the granitic magma.

3. The K-Ar ages of the porphyry copper deposits embedding along the Domeyko Cordillera in northern Chile indicate 30-40Ma(Olson,1989), as shown in Fig.II-1-7.

Although the alteration pattern in the Sierra Overa district is similar to that of the porphyry copper deposits, the period in which the alteration has been formed differs from that of the porphyry copper deposits of the Domeyko Cordillera.

1-2 Trench Survey in the Veraguas District

The Sierra Overa northwest district is made up of aphanitic andesite of the Cretaceous Aeropuerto formation and intrusive diorite porphyry that have undergone hydrothermal alteration, and intrusive dioritic porphyry. The porphyry is distributed over a width of 100-200m in a NW-SE direction, and is thought to be spread in stock form in the deeper part. The alteration is divided, from the top down, into the following zones.

Silicified & siliceous argillized zone: The eastern part of Line 3, on the ridge of the Sierra Overa.

Leached zone with strong concentrations of pulverized reddish hematite, jarosite and natrojarosite, accompanying siliceous clay: The central part of Line 3 and Lines 1 & 2 on the foot of the Sierra Overa.

Chloritized zone : The western part of Line 3 and the eastern part of Line 2, to the north of that.

Cu oxides disseminates and film in the aphanitic andesite and diorite porphyry, belonging to the chloritized zone. Cupper mimerals are chalcanthite, atacamite and small amount of chalcopyrite, bornite accompaning magnetite, hematite and goethite.

Principal component analysis was carried out using the chemical analysis data of the 64 samples. The results were as follows.

(1)First principal component: T.Cu, S.Cu, I.Cu, Au display identical behaviour.

(2)Second principal component: Mo shows independent behaviour.

(3)Third principal component: Au and I.Cu interact.

From the occurrence and the behaviour of the components described above, it is thought that the copper oxides have been formed as secondary mineral from oxidized primary copper sulphides, and that this was accompanied by concentrations of gold.

It is therefore necessary to continue prospecting, in order to ascertain the existence of the secondary enrichment and primary deposits in the deeper part of the Sierra Overa.

1-3 Geophysical survey in the Progreso Area

The results of the 1994 survey made it clear that the Punta del Cobre formation, which is a horizon-type ore deposit, is deep, reaching approximately 470m down from the surface in the southern part of the area. In addition mineral prospects of skarn were found in the limestone of the Abundancia formation above that. On the basis of these results, and in order to elucidate the state of distribution of the Punta del Cobre formation and extract more zones of mineralization, AMT and IP survey was carried out along 5 profile(9,4km), cores were measured their resistivity and polarizability in a laboratory, and PEM survey was carried out at the DDH-1A hole.

The results of the survey did not reveal the areas of anomaly showing low resistivity-high chargeability that had initially been forecast. In the laboratory measurements on boring cores it was found that the samples from this area showing a high chargeability tended on the whole to display a high resistivity. Values measured in samples taken from DDH-1A and DDH-6A, where the Punta del Cobre formation, a horizontal ore deposit, has been verified, displayed high resistivity values of 800Ωm(average resistivity 10,635Ωm). While the lack of boring data actually striking deposits in this area makes it difficult to be certain, it is thought probable that actual Manto-type deposits do have a low resistivity-high chargeability, and it was not possible from the results of this survey to extract any such marked anomaly. However, the high resistivity-high chargeability anomaly either arises from a garnet skarn of the Abundancia formation accompanying mineralization, or the resistivity of the andesite which is the country rock of the Punta del Cobre formation is extremely high and the influence of this was observed in the surface measurements as high resistivity-high chargeability. If this is the case, we cannot expect to find large scale deposits of minerals, but the question can be considered a survey index.

Like the resistivity values for the Punta del Cobre formation, resistivity values for the Abundancia formation, which were verified in DDH-6A, were high, 1,000Ωm or above (average resistivity value 3,510.2Ωm), and it is considered difficult to separate the Punta del Cobre formation from the Abundacia formation using resistivity values. However, as the resistivity values of the alluvials are low and the difference is clear, it is possible to clarify the geologic structure of the survey area by tracing the structure of the high resistivity values. Moreover, looking at the correspondence between the chargeability of core samples and copper analysis values, the high chargeability core samples in DDH-1A have the high copper analysis values.

Taking an overall view of the resistivity structure of this area, the results of the two-dimensional joint inversion analysis show that in the resistivity structure of the whole area there is a tendency for the zone of high resistivity to be shallow on the east side, and deep on the west side. In the north, taking profile II measurement point 1400 as the boundary, the high resistivity zone becomes rapidly deeper on the north side and the existence of a fault is assumed. In the east, the high resistivity zone juts out from profile III measurement point 800 towards profile IV measurement point 2200, and the existence of intrusive rocks is

assumed from this structure. In the south, the high resistivity zone becomes shallow on the south side linking profile V measurement point 500 and profile IV measurement point 800, and then becomes deep again on the south side linking profile V measurement point 1100 and profile IV measurement point 400. From the range of the present measurements it is impossible to ascertain whether this tendency extends over the entire south side of the survey area or is a local drop. The high resistivity zone on the west side from profile V measurement point 200 is shallow. This is an area in which geologically also the Abundacia formation is distributed on the surface, so that both results agree. No anomalies indicating mineral prospects were observed from the results of PEM measurements in DDH-1A.

As described above, anomalies indicating marked mineral prospects with a low resistivity-high chargeability were not found in this area. However, assuming that the high resistivity-high chargeability anomaly indicates a skarn mineral deposit, or indicates a structure in which the Punta del Cobre formation is distributed near the surface and is accompanied by the mineralization effect, the chargeability is over 50mV/V are laid over the a shallow region of a high resistivity zone is thought to be an effective indicator of mineral prospects in this area. From the point of view these regions can be extracted, the region centering on profile II measurement point 1300 in the central eastern part of the area and the region centering on profile III measurement point 1000. In addition, a region with high chargeability centering on profile II measurement point 2000 in the northeast of the area was confirmed. While no rise in the zone of high resistivity is assumed, a region of high chargeability was observed; this is a region close to a high anomaly zone measured in the airborne magnetic survey, and it is hoped that these areas will be subjected to further surveys.

CHAPTER 2 RECOMMENDATIONS FOR PHASE III

On the basis of the results of the Phase I surveys, the following recommendations are made for Phase III.

2-1 Veraguas Area

From this phase of the survey it may be expected that mineral deposits originating in the Cretaceous granitic magma activity and contolled by the NW-SE structure do exist in the Sierra Overa district and the district from the eastern side of the Cerro Veraguas to the Pampa plain, where copper mineralizations were found. In particular it may be expected that porphyry copper type deposits would be embedded under the leached zone that forms the Sierra Overa.

Thus it would be desirable for drilling and trench surveys to be continued over from this year into Phase 3, in the Sierra Overa area indicated on Fig.III-2-1.

2-2 Progreso Area

Anomalies indicating marked mineral prospects with a low resistivity-high chargeability were not found in this area. However, assuming that the high resistivity-high chargeability anomaly indicates a skarn mineral deposit, or indicates a structure in which the Punta del Cobre formation is distributed near the surface and is accompanied by the mineralization effect, a search brings to the fore the region centering on profile II measurement point 1300 in the central eastern part of the area and the region centering on profile III measurement point 1000. In addition, a region with high chargeability centering on profile II measurement point 2000 in the northeast of the area was confirmed. While no rise in the zone of high resistivity is assumed, a region of high chargeability was observed; this is a region close to a high anomaly zone measured in the airborne magnetic survey, and it is hoped that these areas will be subjected to further surveys. Thus it is desirable in Phase 3 for a drilling survey to be carried out in the central-eastern and northeastern parts of the Progreso area indicated on Fig.III-2-2 .

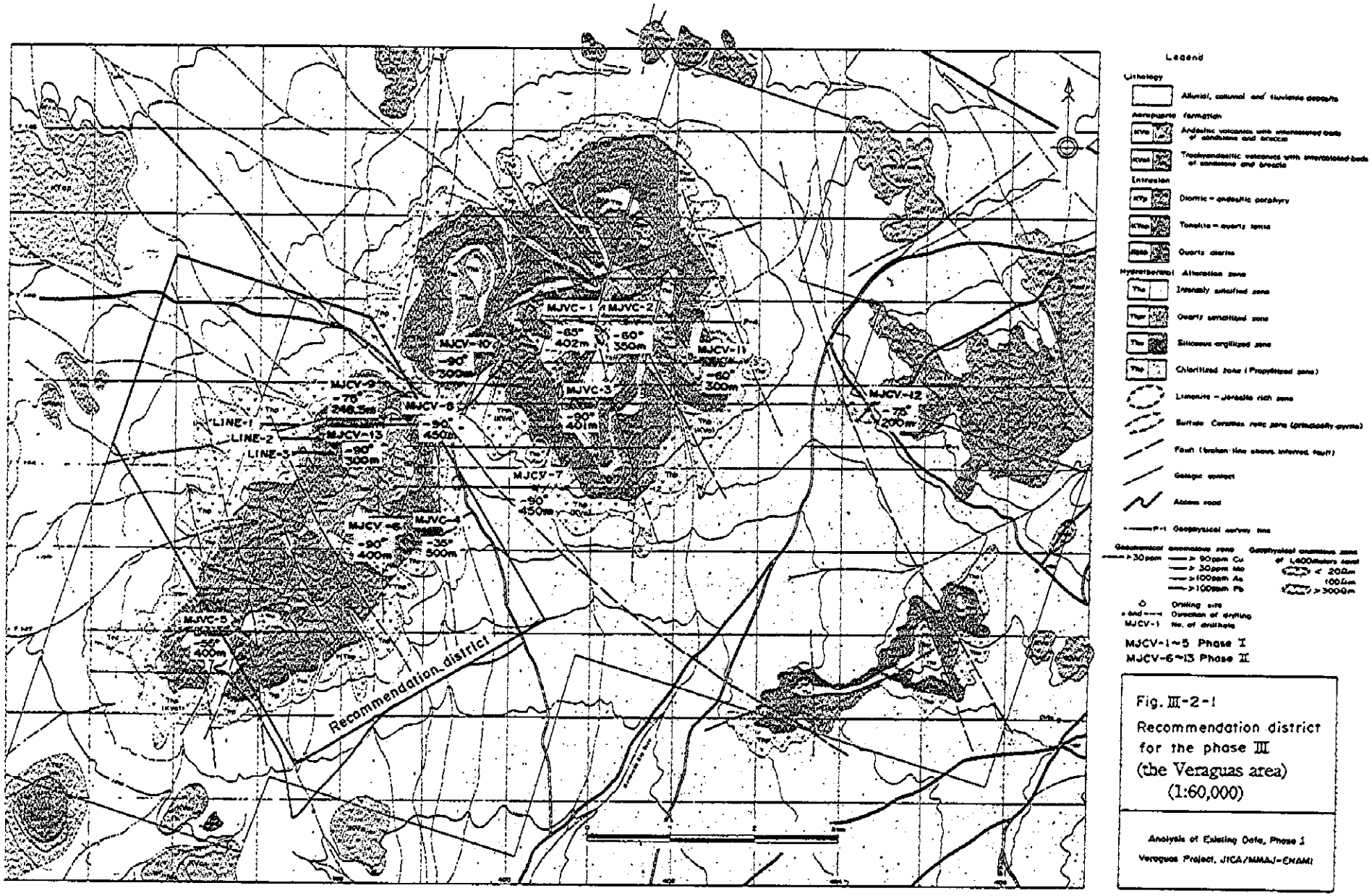

Fig. III-2-1
Recommendation district for the phase III (the Veraguas area) (1:60,000)

Analysis of Existing Data, Phase 1
Veraguas Project, JICA/MMAJ-ENAM

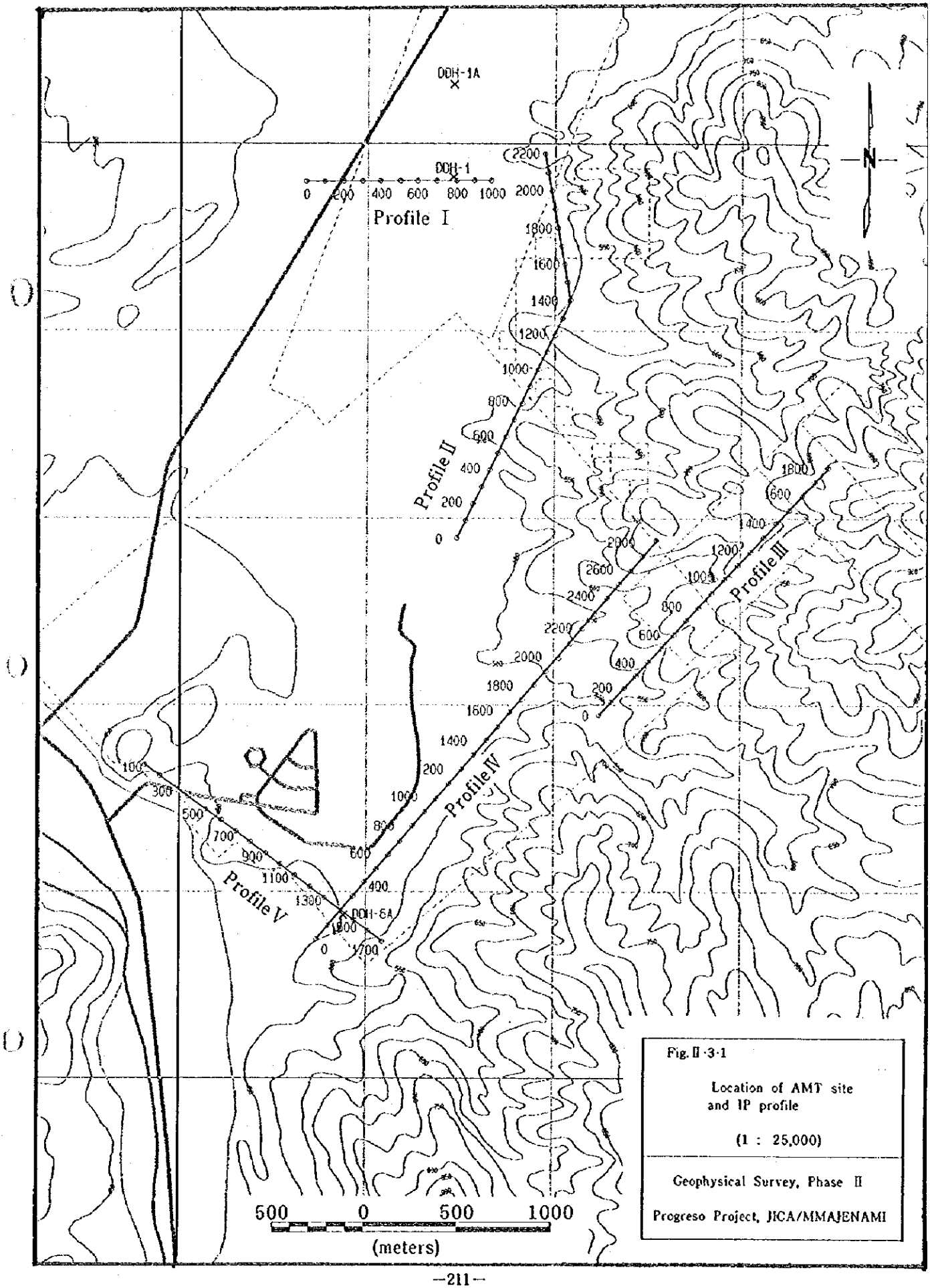

Fig. II-3-1

Location of AMT site and IP profile

(1 : 25,000)

Geophysical Survey, Phase II

Progreso Project, JICA/MMAJENAMI

REFERENCES

REFERENCES

Veraguas Area

<Drilling and Trench Survey>

1. Bell,C.M.(1982): The Lower Paleozoic Metasedimentary Basement of the Coastal Ranges of Chile between 25° 30′ and 27° S; En Revista Geologica de Chile, Numero 17.

2. Boric,r.p.,Diaz,f.f.,,y Maksaev,v.j.(1990):Geologia y Yacimientos Metaliferos de la Region de Antofagasta,Servicio Nacional de Geologia y Mineria-Chile, Boletin No.40.

3. Camus,F. y Duhalde,M.A.(1982): Geologia de los Yacimientos Hidrotermales de Oro en Chile;En Revista Geologia de Chile,Numero 17.

4. Delbridge,C.G.,Robertson,A. and Crozier,R.D.(1992): Mineral Industry Profiles Chile, Delbridge-Robertson Associates.

5. ENAMI(1987): Estudio Geologico-Economico Preliminar del Area de las Pertenencias Mineras Virgo 1-1213 del Distrito Minero de Sierra Overa.

6. ENAMI(1993): Evaluación Geologia Prospecto Cerro Veraguas.

7. ENAMI(1993): Estudio Geofisico Mediante CSAMT Sector Sierra Overa.

8. ENAMI(1993): Levantamiento Topografico Acceso a Sondajes Prospecto Veraguas II Region de Antofagasta Comuna Taltal,Chile.

9. Garrels,R.M. and Chist,C.L.(1965):Solutions,Minerals,and Equilibria. Jones and Bartlett Publishers

10.JICA & MMAJ(1993): An Interm Report of Mineral Exploration in Cerro Negro, The Republic of Chile, Phase I.

11.JMEC(1993): Report on The Project Finding Survey of The Cooperative Mineral Exploration, Satellite Image Interpretation in Veraguas-Progreso area, The Republic of Chile.

12.Lowell,J.D.(1991):The Discovery of the La Escondida Orebody, Ecom. Geol. Monograph 8,pp.300-313

13.Mercado,M.W.(1978):Hojas Chanaral y Potrerillos,Region de Atacama, Geologicos Preliminares de Chile,Escala 1:250,000 Instituto de Investigaciones Geologicas .

14.MMAJ(1972): Ore Deposits in Chile.

15.Naranjo,J.A. y Puig,A.(1984):Hojas Taltal y Chanaral,Region de Antofagasta y Atacama,Carta Geologica de Chile,Escala 1:250,000,Servicio Nacional de Geologia y Mineria.

16.Olson,S.F.(1989):The Stratigrafic and Structural Setting of the Potrerillos Porphyry Copper District,Northern Chile; En Revista Geologica de Chile, vol 16, No.1.

17.Perello,J. y Cabello,J.(1989): Porfidos Cupriferos Ricos en Oro;Una Revisión En Revista Geologica de Chile, vol 16, No.1.

18.Ulriksen,C.G.(1990):Mapa Metalogenico de Chile entre los 18° y 34° S (1:1.000.000),Servicio Nacional de Geologia y Mineria-Chile,Boletin No.42.

Progreso Area

<Geophysical Survey>

1. Boric,R.P(1985): Geologia y yacimientos metalicos del Dristrito Talcuna, IV Region de Coquimbo. Revista Geológia de Chile,no.25.26,p57-58.

2. Corvaland,J.(1973): Estratigrafia del neoconiano marino de la region al sur de Copiapo, Providensia de Atacama. Revista Geológia de Chile,no.1,p13-36.

3. Hopf,S.(1990):The Agustina mine,a volcanic-hosted copper deposit in northern chile. Stratabound ore deposits in the Andes. Springer-Verlag Berlin Heidelberg. p421-434

4. Kenneth Segerstrom(1968):Geologia de las Hojas Copiapo y Ojos del Salado, Provincia de Atacama,Instituto de Investigaciones Geologicas Chile. Boletin No.24

5. Keneth Segerstrom y Carlos Ruiz Fuller(1962):Carta Geologica de Chile, Cuadrangulo Copiapo,Escala 1:50,000 Instituto de Investigaciones Geologicas Chile.

6. Segerstrom,K.(1960): Cuadrángulo Quebrada Paipote, Provincia de Atacama. Santiago,Inst. Invest. Geol.,Carta Geol. Chile, vol.2, no.1

7. Segerstrom,K.,y Parker,R.L.(1959): Cuadrángulo Cerrillos, Provincia de Atacama. Santiago,Inst. Invest. Geol.,Carta Geol. Chile, vol.1, no.2

8. Segerstrom,K.,y Ruiz,C.(1962): Cuadrángulo Copiapó, Provincia de Atacama. Santiago,Inst. Invest. Geol.,Carta Geol. Chile, vol.3, no.1

9. Segerstrom,K.,Thomas,H.,y Tilling,R.I.(1963): Cuadrángulo Pintadas, Provincia de Atacama. Santiago,Inst. Invest. Geol.,Carta Geol. Chile, no.12

10.Tilling,R.I.(1976): El batolito andino de Copiapó, Provincia de Atacama. Geologia y Petrologia Revista Geológia de Chile,no.3,pl-24

11.ENAMI(1992): Informe Geologico Final Proyecto de Estudios Progreso Pertenencias Progreso 1-211 Copiapo, III Rerión, Chile.

13.ENAMI(1993): Estudio Geofisico Mediante CSAMT Y Polarization Inducida. Especial Proyecto Progreso,Copiapo III Region Sector Pan,Progreso Sur Intermedio y Progresosur.

14.ENAMI(1993):Estudio Geofisico Mediante CSAMT Y Polarization Inducida Especial Proyecto Progreso,Copiapo III Region Proyecto Norte.

15.ENAMI(1994):Informe Sobre Tres Sondajes Exploratorios Efectuados En Las Perte nencias Progreso 1-211, Paipote III Region.

16.ENAMI(1994):Estudio Geofisico Mediante CSAMT Y Polarization Inducida Unificac ion Sectores Progreso Y Ladrillo Copiapo-III Region.

17.Misac N.Nabighlan:Electromagnetic Methods in Applied Gepphysics Vol2. Part B Society of Exploration Gephysicists

18.Sternberg,B.K.,Washburne,J.C.,and Anderson,R.G.,(1985):Investigation of MT static shift correction methods. 55th Ann.Interant.Mtg.Soc.Expl.Geophys., Extended abstract, 264-267